Ethosomes-mediated tryptanthrin delivery as efficient anti-psoriatic nanotherapy by enhancing topical drug absorption and lipid homeostasis

Pengyu Wang[1,2†], Shihao Hong[1†], Can Cao[1], Shijie Guo[1], Chen Wang[3], Xi Chen[4], Xinnan Wang[3], Ping Song[5], Ning Li[1*] and Ruodan Xu[1*]

Abstract

Psoriasis is a chronic, relapsing, and refractory immune-mediated skin disease with the etiology and pharmaceutical targets remaining unsatisfactorily addressed. Topical herbal-derived compounds, such as tryptanthrin (Tryp), have been considered as an alternative therapy for psoriasis due to their lower costs and fewer side effects compared to other therapies. However, the effectiveness of topically administered drugs is substantially limited by the thickened pathological skin barrier and the low bioavailability of drugs in the deeper layers of the lesion. Ethosomes, being a novel phospholipid-based vesicle system with high content of ethanol, have been implicated in enhancing topical drug absorption and restoring psoriatic lesions. In this study, taking advantages of ethosomes as a soft and malleable drug carrier, we constructed the Tryp-loaded ethosome (Tryp-ES) through a one-step microfluidics-based technique. The optimal formulation of Tryp-ES was achieved by adding amino-acid-derived surfactant sodium lauroyl glutamate, and Tryp-ES exhibited homogeneous particle size and favorable stability at room temperature. In vitro evaluations showed that Tryp of Tryp-ES could be easily internalized into cells and accumulated in cell nuclei, hence inhibited the abnormally proliferated keratinocytes by inducing apoptosis. In vivo and in vitro assessment using psoritic skin of mice revealed that Tryp-ES had preferred skin retention and permeation of loaded drugs within the initial 1 h of topical administration, which could be attributed to transient disintegrations of cell membranes by ethosomes, thus improved cellular fluidity and permeability. Notably, a synergistic effect of ethosomes and Tryp was found in psoriatic mice. Tryp-ES-treated mice showed substantially ameliorated symptoms of psoriasis and reduced pathological alterations due to hyperplasia, inflammation and angiogenesis, without detectable local or systemic toxicities. Interestingly, lipidomics analysis confirmed that the supplementation of phospholipids, as in the form of ethosome vehicles, was an alternative strategy to relieve psoriatic pathologies.

†Pengyu Wang and Shihao Hong contributed equally to this work.

*Correspondence:
Ning Li
lili.li.ning@gmail.com
Ruodan Xu
ruodanxu@gmail.com

Full list of author information is available at the end of the article

Taken together, this study provides a novel impact for ethosomal topical delivery of Tryp and underlines their potential as an effective therapy for the management of psoriasis.

Keywords Ethosomes, Tryptanthrin, Anti-psoriasis, Topical delivery, Microfluidics

Introduction

Psoriasis, a refractory disease defined by WHO, is a chronic immune-mediated inflammatory skin condition, affecting 2–4% of the population globally [1–3]. It typically manifests as erythematous plaques covered with white scaly flakes and causes dryness, pain, and itching [4]. Although the exact etiology of psoriasis remains unclear, it is widely accepted that aberrant keratinocyte proliferation, blood vessel dilation and overactivation of immune cells in the dermis are responsible for the pathogenesis of psoriasis. Currently, the exact pharmaceutical targets and corresponding interventions for psoriasis remain unsatisfactorily addressed [1, 5–7]. Topical medication is generally regarded as the first-line therapy in mild to moderate localized psoriasis due to the reduced systemic absorption of potentially toxic drugs, thereby avoiding systemic adverse effects [4, 8]. However, the skin barrier of stratum corneum (SC) limits the therapeutic molecules being percutaneously absorbed, causing drug wastage and poor clinical efficacy.

Various technologies have been studied to enhance drug topical delivery through physical or chemical approaches, such as ultrasound, ultraviolet light and nano-carriers [9, 10]. Among nanocarriers, ethosomes as a novel phospholipid-based vesicle system with a high content of ethanol, have demonstrated a unique improvement in drug delivery for treating melanoma and other skin diseases [11, 12]. The significance of phospholipids in lipid nanocarrier systems has been largely attributed to their involvement in the formation of cellular membranes and skin barriers [13]. For instance, one such phospholipid, dimyristoylphosphatidylcholine (DMPC), is often employed to prepare liposomes or ethosomes due to its biocompatibility with human tissues [14]. Previous studies have suggested that lipid abnormalities in the skin may lead to impaired skin barrier and increased skin inflammation [15, 16], whereas supplementation with phospholipids could help to alleviate the skin inflammation associated with psoriasis [17–19]. Moreover, the high contents of ethanol in ethosomes generally offer this vehicle soft and malleable characteristics, which permit ethosomes to easily squeeze through smaller skin pores and intercellular spaces. The increased fluidity of the skin's lipid bilayers by ethanol consequently allows an in-depth penetration of the nanovesicles. However, in practical applications, the utilization of ethanol is highly associated with skin irritability and dermatitis, which makes it unsuitable for psoriasis-affected skin [20]. Propylene glycol, which is characterized by low toxicity and irritancy, minimal volatility, and stable physicochemical properties with superior moisture retention, can be used as an alternative in ethosomes formulation [21]. In particular, previous studies have demonstrated that propylene glycol-mediated liposomes exhibited superior drug deposition in the skin compared to conventional liposomes and ethanol-formed ethosomes [22]. The more advanced application of the ethsosomes has led to a broad conceptualization that extends beyond the conventional use of high-content ethanol. This encompasses the utilization of other low molecular-weight alcohol solvents, including propanediol, isopropanol, and combinations of these solvents [23]. Besides, lauroyl glutamate sodium (LGS) has been additionally used to improve the stability of ethosomes by adjusting their size and charge properties [24]. As an amino-acid-derived surfactant, LGS is also commonly applied to soften the phospholipid membrane and increase the deformability of nanocarriers for topical delivery.

The on-chip microfluidics provides a new possibility for the synthesis of lipid-based nanoparticles such as liposomes [25]. This microfluidic approach involves the application of various geometries of the mixing channel as well as the use of shear forces, electric fields and other microfluidic effects that occur in the channel [26]. In our previous study, by using microfluidics and phospholipids, we reported the construction of peptide-based high-density lipoprotein (pHDL) and the pHDL loaded with lipophilic compounds, such as curcumin and TanIIA [27, 28]. We further demonstrated the ability of microfluidics to control the mixture process of organic and water phases, with the production of structurally and morphologically homogenous nanoparticles [27, 28].

Tryptanthrin (Tryp) is the main active component found in *indigo naturalis*, which is a traditional herbal medication derived from *Indigofera tinctoria* and other indigo plants' leaves and stems. Previous studies indicate that Tryp can alleviate imiquimod (IMQ)-induced psoriatic mice by suppressing inflammation and oxidative stress via NF-κB/MAPK/Nrf2 pathways [29]. Additionally, Tryp has anti-angiogenesis effects by inhibiting the promoter activity of the apelin gene expression and reducing mRNA stability in endothelial cells [30]. Our previous study further confirmed that Tryp played a critical role in suppressing cell proliferation and angiogenesis [31]. Despite its numerous pharmaceutical values, the low solubility and dispersibility of Tryp result in poor topical availability. Consequently, the formulation of Tryp as a therapeutic drug and the overcoming of

the difficulties in penetrating the SC remain significant challenge.

In the current study, with the microfluidic device, we developed a functionalized ethosomal drug delivery nanovehicle encapsulated with Tryp as a topical treatment for psoriasis. The optimized Tryp-loaded ethosomes (Tryp-ES) were obtained in a microfluidics formulation generated through the hydration method. With the facilitation of ethosomes in tissue penetration, Tryp could exert its anti-psoriatic activities in the deeper layers of psoriatic skin, leading to significantly reduced skin lesions and pathological changes of psoriasis. Further lipidomics analysis revealed that the supplementation of phospholipids, as the form of ethosome vehicles, was an alternative strategy to relieve psoriatic pathologies. Our functional Tryp-ES formulation provides a new therapeutic option for the topical treatment of psoriatic lesions and offers new evidence for the application of ethosomes in the field of topical delivery.

Materials and methods
Materials
Tryp (≥98% purity) and LGS were purchased from Yuanye Bio-Technology (Shanghai, China). 1,2-dimyristoyl-sn-glycero-3-phosphocholine (DMPC) and 1,2-dimyristoyl-sn-glycero-3-phospho-rac-[1-glycerol] (DMPG) were obtained from Avanti Polar Lipids, Inc. Propanediol, triethanolamine, ethyl acetate and carbopol were supplied by Aladdin Biochemical Technology (Shanghai, China). Methanol (HPLC and MS grade), acetonitrile (MS grade) and isopropanol (HPLC grade) were purchased from Thermo Fisher Scientific (Fair Lawn, NJ, USA). Methyl tert-butyl ether (MTBE), formic acid (HPLC grade) and ammonium formate (HPLC grade) were obtained from Sigma-Aldrich (St. Louis, Mo, USA).

Synthesis of Tryp-loaded ethosomes and Tryp-loaded ethosome gel
Tryp-ES were synthesized using a polydimethylsiloxane (PDMS) microfluidic chip, which comprises three inlets and one outlet (Wenhao Co. Ltd, Suzhou, Jiangsu, China). Briefly, Tryp-ES were prepared by injecting into the middle channel of the microfluidic chip a mixture of DMPC (5–15 mM) with Tryp dissolved in propanediol (0–100 μg/mL) at a rate of 200–400 μL/min. Solutions of LGS in double-distilled water (ddH$_2$O, 0.01–0.03% w/v) were injected into the two external channels at a rate between 300 and 400 μL/min for the optional strategy. The resulting products were collected from the outlet channel.

Gel carrier of empty ethosomes or Tryp-loaded ethosomes (Tryp-ES gels) were prepared using 1.5% (w/v) carbopol, 5% (w/v) propanediol, 1.5% (w/v) triethanolamine, and distilled water with or without Tryp-ES consisting of 0.00075% (w/v) Tryp. Initially, a homogeneous solution consisting of distilled water, ES or Tryp-ES solutions, and propanediol was prepared in specific proportions. When preparing various doses of ethosome gels, the total volume of the solution was adjusted to 3, 6, and 9 mL, respectively. Carbopol powders were then evenly dispersed into the solution and allowed to swell gradually and uniformly overnight at 4 °C. The following day, triethanolamine was added to neutralize the carbopol and achieve a pH of approximately 5.3 to facilitate stable gel formation. Simultaneously, the mixture was vigorously stirred to ensure even distribution of the triethanolamine and initiate the gelation process, yielding the empty ethosomes gels and Tryp-ES gels.

Determination of particle size, polydispersity index (PdI) and zeta-potential
The particle size (weighted by intensity), PdI and zeta-potential of the prepared ethosome formulations were measured using Malvern Zetasizer Ultra (Malvern Panalytical Ltd., Malvern, UK) at 25 °C. All the batches were diluted with Milli-Q ultrapure water (Millipore, Molsheim, France) at 1:10 dilution and analyzed. All measurements were performed in three parallel replications.

Transmission electron microscopy (TEM)
The morphology of the ethosomes or Tryp-ES was characterized by transmission electron microscopy (TEM). For TEM, 10 μL samples were added to a carbon-coated copper grids (Beijing Zhongxing Bairui Technology Co., Ltd., Beijing, China), then negatively stained with 10 μL 2% sodium phosphotungstate (Yuanye Bio-Technology, Shanghai, China). Once stained and air-dried, the images were taken with a Hitachi H7650 TEM microscope (Tokyo, Japan) at 80 kV.

Atomic force microscopy (AFM)
The surface topography of prepared ethosomes was analyzed by AFM Cypher ES (Asylum Research, Oxford Instruments, Santa Barbara, CA, USA). Briefly, samples were dropped onto 10 mm mica discs (TedPella, USA) and vacuumed dry at room temperature (RT) for 2 h. Scanning was performed in AC Air Topography mode using AC200TS-R3 probe (Olympus, Japan) with a constant of 9 N/m at a temperature of 25±1 °C.

The influence of prepared ethosomes on the morphology of DMPC and DMPG (4:1) bilayers was examined by AFM Cypher ES. A solution of DMPC (2 mM) and DMPG (0.5 mM) in anhydrous ethanol was quickly mixed and sonicated for 30 min at RT. The mixture was deposited onto freshly cleaved mica and incubated at 40 °C for an hour. The surface was rinsed three times, and the bilayers were imaged in the buffer by the addition of 800 μL ethosomes over the supported bilayers.

Scanning was performed in AC Water Topography mode using an AC160TSA-R3 probe (Olympus, Japan) with a spring constant of 26 N/m and a resonance frequency of 300 kHz. The membranes samples were scanned at a rate of 1.7 Hz, with a drive frequency of 125 ± 5 kHz, and a resolution of 512×512 pixels. The images were analyzed using Asylum Research Real Time software (v.18.04.23).

High-performance liquid chromatography (HPLC)

The concentration of Tryp in the samples was quantified by an Agilent 1100 HPLC system equipped with a UV detector (Agilent Technologies, Palo Alto, CA, USA). In chromatography, the C18 column (Agilent, Stable Bond 300, 250 mm × 4.6 mm, 5 μm) was used with a methanol/ddH$_2$O mobile phase (60:40, v/v) at a flow rate of 1 mL/min. The amount of Tryp was quantified at 254 nm, with a retention time of 5.5 min. The peak of Tryp was successfully distinguished from other peaks in the chromatogram, demonstrating no interference from the other peaks. The concentration of Tryp was determined by means of a calibration curve spanning the range from 0.01 to 10.0 μg/mL. The same concentration solutions of Tryp standards were subjected to analysis on three consecutive occasions using the established HPLC method. In all cases, the relative standard deviation (RSD) was less than 3.0%, which fulfills the technical requirements for an HPLC chromatogram.

Entrapment efficiency (EE)

The prepared samples were centrifuged at 1000 rpm, 4 °C for 2 min to separate the unencapsulated drug. The supernatant was collected and then treated with 0.1% Triton X-100 (Sigma) to disrupt the ethosomes. All samples were filtered through a 0.45 μm membrane (Millipore, Billerica, MA, USA) before HPLC analysis. The entrapment efficiency (EE) was calculated according to the following equation:

$$\text{Entrapment efficiency } (\%) = \text{Ts/Tp} \times 100,$$

where Ts is the content of Tryp loaded in the formulation, and Tp is the initial content of Tryp added in the formulation.

Stability evaluation of ethosomes

Tryp-ES were stored at 4 ± 1 °C or 25 ± 1 °C (RT) for 28 days. Both the physical and the chemical stability of Tryp-ES were evaluated. The physical stability was assessed by visual observation, particle size, PdI, and zeta potential determination. The chemical stability was determined by measuring the content of Tryp encapsulated in ethosomes by HPLC on days 1, 7, 14, 21 and 28. The physical evaluation of gel appearance, pH, and drug content was conducted over a period of 28 days at 4 °C

and 25 °C for all prepared gel formulations. The pH of the Tryp-ES gel was determined using a Sartorius PB-10 pH meter (Sartorius, Germany). Briefly, 1 g of Tryp-ES gel was dissolved in 100 mL of ultrapure water, and the solution was tested in triplicate, with the average value calculated. Prior to analysis of the drug content, the gels were diluted with ultrapure water in a 1:100 ratio (gel: ultrapure water=1:100). The drug content was analyzed by HPLC, as described above.

In vitro drug release

The Tryp release profile from Tryp solution, Tryp-ES and Tryp-ES gel were assessed using the dialysis bag (3500 MWCO, Biorigin, Beijing, China) diffusion method in a 40 mL solution with 10% propanediol at 32 ± 1 °C. For a period of 48 h, 1 mL of solution was collected from each sample at 10, 20, 30 min and 1, 2, 4, 8, 12, 24, 48 h, while 1 mL fresh solution was added to each sample to maintain a constant total volume of 40 mL. The amount of released Tryp was analyzed by HPLC.

Skin permeation and retention studies

The in vitro skin permeation and retention of Tryp from Tryp-ES were investigated using Franz type glass diffusion cells as previously described in detail [31]. Specifically, the dorsal skin of psoriatic mice treated with 62.5 mg IMQ cream daily on the exposed dorsal skin for 7 days was excised, the subcutaneous fat was carefully removed, and the skin was mounted with the SC facing up on a Franz type glass diffusion cell (Huke, Jiangsu, China) with an effective area of 3.14 cm². Briefly, excised psoriatic mouse skin was mounted between the donor and receptor compartments with the dorsal surface of the skin facing up into the donor chamber. Tryp solution, Tryp gel, Tryp-ES or Tryp-ES gel were applied onto the skin in the donor chamber without sealing. The receptor chamber was filled with 10% propanediol and stirred with a magnetic bar at 200 rpm to equilibrate at 32 ± 1 °C. At time intervals of 0, 10, 20, 30, 40, 50 and 60 min, or 2, 4, 8, 12 and 24 h, a 1 mL aliquot of receptor was collected, and the same volume of fresh medium was added back. The amount of Tryp in the samples was analyzed by HPLC, and the cumulative amount was plotted against time. The permeation of drug was calculated according to the following formula.

Permeation of drug (%) = (amount of permeated drug/ initial amount of drug) $\times$ 100.

For the drug retention assay, skin samples were collected from the donor chamber at 1 h, or 2, 4, 8 and 24 h. The epidermis was separated from the dermis under the condition of 0.125–0.25% trypsin-EDTA (Gibco, Grand Island, NY, USA) at 25 or 37 °C for 0.5–2 h (Table S1) and tissue samples were ground using a cryogenic grinder (JXFSTPRP-II, Jingxin Industrial Development Co., Ltd.,

Shanghai, China). After extraction of Tryp from skin tissues with ethyl acetate three times, the samples were concentrated under vacuum. The precipitate was dissolved in 200 µL DMSO (Aladdin) for further HPLC analysis.

Skin biodistribution studies
Rhodamine B (0.01%, w/v, Sigma-Aldrich) loaded ethosomes (RhB-ES) were prepared using the microfluidic device described in the synthesis of Try-ES. The method used for preparing Rhodamine B ethosomal gel (RhB-ES gel) was identical to that used for Tryp-ES gel. RhB-ES or RhB-ES gel with the same dose of rhodamine B was applied topically to the dorsal skins of IMQ mice. At 0, 10, 20, 30 and 60 min, the back skin of the mice treated with RhB-ES and RhB-ES gel was cut off and embedded in the optimal cutting temperature compound (Sakura Finetek, Torrance, California, USA). After being snap-frozen in liquid nitrogen, the tissue was sectioned at 8 µm. The penetration and biodistribution of RhB-ES and RhB-ES gel of different skin layers were evaluated by confocal laser scanning microscopy (Olympus FV3000, Tokyo, Japan).

Cell culture
Human keratinocytes (HaCat) were cultured in RPMI-1640 medium (Gibco) containing 10% fetal bovine serum (FBS, Gibco) and 1% penicillin/streptomycin (P/S, Gibco). Human umbilical vein endothelial cells (HUVEC) were cultured in complete endothelial cell medium (ECM, ScienCell, San Diego, CA, USA) supplemented with 10% FBS (ScienCell), 1% endothelial cell growth supplement (ECGS, ScienCell) and 1% P/S (ScienCell). All cells were cultured in a humidified 5% CO_2/37 °C incubator. Cells were regularly passaged every 5–7 days with 0.25% trypsin-EDTA (Gibco).

Cell proliferation
Cell proliferation was assayed using CellTiter96® Aqueous One Solution Cell Proliferation Assay Kit (Promega, Madison, WI, USA). Briefly, HaCat cells were seeded at a density of 1.5×10^4 cells/cm^2 and cultured with growth medium supplemented with EGF or KGF (0–160 ng/mL) (Abcam, Cambridge, MA, USA) and various concentrations of Tryp solution or Tryp-ES as indicated for 24 h. The cells were then washed by replacing the culture medium with MTS reagent for 3 h. 100 µL of the solution was transferred into a 96-well plate, and the absorbance was measured at 490 nm. The same volumes of culture medium and MTS reagent without cells were also incubated as the background.

In vitro cellular uptake
Cellular uptakes of Tryp-ES or Tryp solution was assessed using the intrinsic fluorescence properties of Tryp with a fluorescence microscope. HaCat cells were seeded in 12-well plates at a density of 6.5×10^3 cells/cm^2. When the cells confluence reached 80%, they were washed and incubated with Tryp-ES or Tryp solution at an equivalent Tryp dose of 300 ng/mL for 1, 3, 6, 12 and 24 h. The cells were then washed three times and fixed with 4% paraformaldehyde (Solarbio, Beijing, China). The samples were permeabilized with 0.2% Triton X-100 and blocked with 1% bovine serum albumin (BSA, Sigma) in PBS for 1 h. F-actin and nuclei were stained with Alexa Fluor 488 Phalloidin (Thermo Fisher Scientific) and DAPI (Abcam), respectively. After washing with PBS, the red fluorescence of Tryp in cells was visualized using the confocal laser scanning microscopy (Olympus) with a 100 × oil immersion objective (numerical aperture 1.4) at 568 nm laser. The z-stack images were then processed as mean intensity projection using FV31S-SW software (v.2.3.2, Olympus).

TUNEL assay
Terminal deoxynucleotidyl transferase dUTP nick end labeling (TUNEL) assay was performed using CoraLite® Plus 488 TUNEL Apoptosis Detection Kit (Proteintech, USA) according to the manufacturer's recommended protocol. HaCat cells were seeded at a density of 2.5×10^4 cells/cm^2 on 24-well plate and incubated overnight to reach 60% confluence. Then, cells were treated with EGF (20 ng/mL) and various concentrations of Tryp-ES or Tryp solution as indicated for 24 h. Following fixation with 4% paraformaldehyde and permeabilization with 0.2% Triton X-100, the TUNEL reaction solution was added and incubated at 37 °C in the dark for 1 h. Before detection, cells were washed three times and counterstained with DAPI to label all nuclei. The fluorescence in the cells was observed using a confocal laser scanning microscope (Olympus).

Tube formation assay
To analyze the angiogenic activity of Tryp-ES, the extracellular matrix (ECM) gel-based capillary tube formation assay was used. This was performed following the manufacturer's instructions. Briefly, HUVECs at a density of 7×10^3 cells/well were seeded on top of matrigel (R&D Systems, MN, USA) coated angiogenesis µ-slides (Ibidi GmbH, Gräfelfing, Germany) at 37 °C. The cells were applied with the treatment of 50 ng/mL recombinant human FGF-basic (bFGF, R&D) or various concentrations of Tryp-ES as indicated in the presence of bFGF for 6 h at 37 °C in a humidified atmosphere with 5% CO_2. Cells were stained with Alexa Fluor 488 Phalloidin and DAPI, and the level of capillary tube structure formation was photographed using Zeiss Axio Observer microscope (Göttingen, Germany) and quantified via the AngioTool (v 0.6a, 64 bits) analysis software.

In vivo animal study

BALB/c mice (male, 6–8 weeks of age, 20±2 g) were purchased from Beijing Vital River Laboratory Animal Technology CO., Ltd. (Beijing, China). All animals were group-housed together with free access to food and water in a controlled experimental environment with a consistent temperature/humidity and a standard light/dark cycle. All animal experiments were performed in compliance with the National Guidelines for Care of Laboratory Animals and approved by the Institutional Animal Care and Use Committee of the Institute of Basic Theory for Chinese Medicine, China Academy of Chinese Medical Sciences.

IMQ, a TLR7/8 ligand and potent immune activator, produces a psoriasis-like cutaneous phenotype in mice, frequently studied as the model of human psoriasis. The mice were divided into 15 groups mice ($n=3$): one group is normal (non-treated group), one group was treated with IMQ (model group) to create the prosiasis-like condition, and the remaining groups were also treated with IMQ but given various treatments, including clobetasol propionate (CP, positive control group), single, double and triple dosing of ethosome vehicle (EV_1, EV_2, EV_3), and single, double and triple dosing of Tryp-ES (Tryp-ES_1, Tryp-ES_2, Tryp-ES_3), as well as those formulations in gel (EV_1 gel, EV_2 gel, EV_3 gel, Tryp-ES_1 gel, Tryp-ES_2 gel and Tryp-ES_3 gel). The ethosome vehicle contained 1 µM DMPC, while the Tryp-ES contained 1.5 µg Tryp loaded into the ethosome vehicle as a single dose. The model group was induced by local administration of 62.5 mg IMQ cream to the dorsal skin once every day for 7 days. Based on the response and tolerability of mice to the tested formulations in pilot studies, ethosome solutions or gels were topically applied to the lesion area of the skin one to three times a day for 20 min each time. The mice were weighed daily, and photographs of the dorsal skin were captured. On the 8th day, all groups were humanely euthanized, and the dorsal skin, liver, kidney, and spleen samples were collected. Blood was taken and stored at 4 °C overnight and then centrifuged at 3000 rpm, 4 °C for 15 min to obtain the serum. Levels of Alanine aminotransferase (ALT), aspartate aminotransferase (AST), albumin (ALB), globulin (GLB), creatine kinase (CK), lactate dehydrogenase (LDH), blood urea nitrogen (BUN) and creatinine (CR) were determined using automatic biochemical analyzer (TBA-40FR, TOSHIBA, Tokyo, Japan) to assess potential toxicity in the liver, heart, and kidneys.

Evaluation of the severity of psoriatic skin lesion

The severity of inflammation on the mice dorsal skins was assessed using the clinical Psoriasis Area and Severity Index (PASI), an objective scoring system was used to evaluate the severity of inflammation [32]. Erythema and scaling scores were obtained daily by blindly scoring with a scale from 0 to 4 (0-none; 1-slight; 2-moderate; 3-marked; 4-very marked). The scores for the scaling and erythema were combined to calculate a total score ranging from 0 to 8, which was assessed once daily for 7 days post-administration.

Hematoxylin and eosin (H&E) staining

Fresh tissues (skin, liver, spleen and kidney) collected from mice were fixed in 4% paraformaldehyde for 48 h. Samples were sequentially subjected to gradient ethanol dehydration and transparent treatment in Histo-Clear (National Diagnostics, GA, USA). Then, the samples were embedded in paraffin, and sectioned into 4-µm slices using a microtome (Leica, Nussloch, Germany). After dewaxing and rehydration, the tissue sections were stained with hematoxylin-eosin staining solution (Solarbio) to identify tissue cytoplasm structures (pink) and distinct nuclei (blue-violet). Images were captured using the Aperio Versa 8 tissue imaging system (Leica, Germany) with an image analysis system (Aperio V.12.4).

Immunohistochemistry (IHC)

For IHC staining, the hydrated sections were subjected to antigen retrieval in citrate buffer (Beyotime, Shanghai, China) at 95 °C for 15 min and cooled down until RT. After inactivating endogenous peroxidase, nonspecific binding sites were blocked with 5% goat serum. Samples were incubated with primary anti-Ki67 (ab16667, 1:400), anti-CD31 (ab124432, 1:1000), anti-CD3 (ab16669, 1:500) from Abcam overnight at 4 °C, followed by incubation with goat anti-rabbit secondary antibody (Zhongshan Golden Bridge Biotechnology, Beijing, China) for 30 min at RT. The positive staining was detected by using diaminobenzidine (DAB) (Zhongshan Golden Bridge Biotechnology) and the nuclei were counterstained with hematoxylin. Images were captured by Aperio Versa 8 scanner and analyzed by ImageJ software v 1.53a (NIH, Bethesda, MD, USA).

Lipidomic analysis

Lipids were extracted from mouse skin tissue using the MTBE method. Briefly, 300 mg of skin tissue was weighed and homogenized with 200 µL water and 240 µL methanol. Then, 800 µL MTBE was added and the mixture was sonicated at 4 °C for 20 min, followed by 30 min exposure at RT. The solution was centrifuged at $14{,}000 \times g$ for 15 min at 10 °C, and the upper organic solvent layer containing the lipids was collected and dried under nitrogen.

The LC-MS analysis was performed with UHPLC Nexera LC-30 A (Shimadzu, Japan) equipped Q Exactive Plus High-Resolution Mass Spectrometer (Thermo Scientific, USA). For UPLC analysis, a CSH C18 column (1.7 µm, 2.1×100 mm, Waters, USA) was used. The lipid extracts
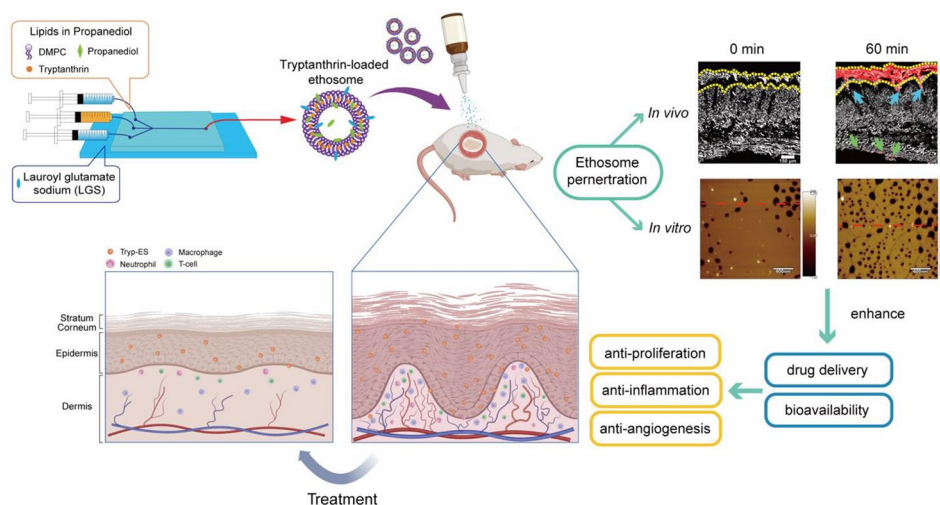
Scheme 1 Schematics of the preparation of Tryp-ES by one-step microfluidics for topical application in psoriatic mice. The anti-psoriasis efficacy is improved by extending drug retention and facilitating drug penetration

Table 1 Characterization of ethosomes with different channel flow rates

Middle channel flow rate (µL/min)	External channel flow rate (µL/min)	1,2-Propanediol (v/v) %	Mean size (nm)	Polydispersity index	Zeta potential (mV)
200	400	20	115.10 ± 15.23	0.28 ± 0.06	-5.82 ± 3.4
300	350	30	122.70 ± 18.51	0.27 ± 0.06	-6.10 ± 5.2
400	300	40	196.90 ± 3.76	0.32 ± 0.05	-4.80 ± 6.4

were re-dissolved in 200 µL 90% isopropanol/acetonitrile, then centrifuged at 14,000 × g for 15 min to obtain the supernatant. A linear gradient consisting of acetonitrile-water (60:40, v/v) with 0.1% formic acid and 0.1 mM ammonium formate (mobile phase A) and acetonitrile-isopropanol (10:90, v/v) with 0.1% formic acid and 0.1 mM ammonium formate (mobile phase B) was used with a gradient program. The injection volume was 3 µL, the flow rate was 300 µL/min, and the column temperature was maintained at 45 °C. Mass spectra were acquired by Q Exactive Plus in positive and negative mode, respectively. Detailed ion source (ESI) parameter settings included: Heater Temperature 300 °C, Sheath Gas Flow rate 45 arb, Aux Gas Flow Rate 15 arb, Sweep Gas Flow Rate 1 arb, spray voltage 3.0 kV, Capillary Temp 350 °C, S-Lens RF Level 50%, MS1 scan ranges: 200–1800. The mass spectrometry data were collected using LipidSearch v. 4.2 (Thermo Scientific, USA) software. After analysis, a data matrix containing lipid molecule identification and quantification was obtained.

The original data were further analyzed and filtered using Python (v. 3.12, Python Software Foundation). To obtain group clustering, supervised partial least squares discriminant analysis was performed on the data. Fold change (FC) was detected using univariate analysis and t-test analysis was performed to calculate P value. To identify patterns and significant differences in lipid metabolite expression profiles among the different treatment groups, principal component analysis (PCA) and volcano plots were generated using the scikit-learn library (v. 1.4.1) and matplotlib (v. 3.8.2). Differential metabolites between the two groups in volcano plots were based on VIP > 1, FC > 1.5 or < 0.67, and $p < 0.05$.

Statistical analysis
Data are expressed as mean ± the standard error of the mean (SEM) and were evaluated using one-way analysis of variance (ANOVA) followed by Bonferroni post hoc test. Statistical significance was defined as $p < 0.05$. All statistical analyses were processed and figures were generated using GraphPad Prism 9.0 (GraphPad Software, Inc., San Diego, CA, USA).

Results and discussion
Preparation and optimization of Tryp-loaded ethosomes
The Tryp-ES was fabricated by employing DMPC lipids, Tryp and LGS in a one-step microfluidic approach, as illustrated in the schematic diagram (Scheme 1). The optimal compositions and parameters were determined through a series of experiments. Initially, 30% propanediol, corresponding to a flow rate of 350-300-350 µL/min (external-middle-external) was chosen due to the smaller PdI (0.27 ± 0.06) and lower zeta potential (-6.10 ± 5.2 mV) of the products (Table 1). Next, at a constant flow rate of 350-300-350 µL/min (external-middle-external), DMPC at 10 mM was selected due to the smaller particle

Table 2 Characterization of ethosomes with different concentrations of DMPC

1,2-Pro-panediol (v/v) %	DMPC (mM)	Mean size (nm)	Polydispersity index	Zeta potential (mV)
30	5	134.80±50.89	0.31±0.18	-13.80±8.88
	10	111.00±29.78	0.32±0.12	-14.21±3.21
	15	114.90±24.36	0.28±0.12	-9.62±12.96

Table 3 Characterization of ethosomes with different percentages of LGS

1,2-Pro-panediol (v/v) %	DMPC (mM)	LGS (w/v) %	Mean size (nm)	Polydispersity index	Zeta potential (mV)
30	10	0.01	109.30±14.31	0.22±0.03	-10.84±6.57
		0.02	107.30±13.61	0.18±0.05	-11.45±3.72
		0.03	112.00±3.74	0.22±0.03	-10.09±1.87

Table 4 Characterization of ethosomes encapsulated with various amounts of Tryp and different percentages of LGS

Tryp (μg/mL)	LGS (w/v) %	Mean size (nm)	Polydispersity index	Zeta potential (mV)
12.5	0	118.00±3.40	0.26±0.03	-4.37±3.00
12.5	0.03	96.94±3.98	0.17±0.03	-15.62±2.51
25	0	94.55±4.83	0.23±0.05	-10.62±5.38
25	0.03	97.06±4.74	0.19±0.04	-13.03±2.94
50	0	93.97±6.04	0.25±0.06	-3.44±2.27
50	0.03	99.93±1.74	0.17±0.03	-13.27±1.36
75	0	107.60±15.60	0.27±0.10	-6.87±2.22
75	0.03	100.10±6.24	0.14±0.04	-16.00±1.86
100	0	97.65±12.14	0.30±0.10	-5.47±2.02
100	0.03	94.70±6.11	0.11±0.02	-15.15±3.37

size (111.00±29.78 nm) and larger negative potential (-14.21±3.21 mV), as shown in Table 2. After optimizing the parameters of propanediol and DMPC, we fixed 0.03% (w/v) LGS since it resulted in much more stable or uniform particle size (112.00±3.74 nm), PdI (0.22±0.03) and zeta potential (-10.09±1.87, Table 3). To further demonstrate the importance of LGS in influencing the synthesis of drug-loaded ethosomes, the Tryp-ES produced by different concentrations of Tryp with or without LGS was evaluated. The results further showed that the formulation containing 0.03% LGS was the most favorable condition to produce uniform and stable ethosomes and ethosomes containing Tryp, mainly based on PdI and zeta potential (Table 4). PdI is an important index of particle size distribution, and the smaller the value of PdI, the more uniform the particle size distribution. Meanwhile, zeta potential reflects the surface charge of the particles and the stability of the ethosomes, and a higher absolute value of zeta potential (either positive or negative) usually means that the system is more stable because the electrostatic repulsive forces between the particles are stronger,

effectively preventing aggregation. As shown in Table 4, when the encapsulated Tryp was 12.5 μg/mL, 25 μg/mL, 50 μg/mL, 75 μg/mL and 100 μg/mL, PdI remained lower in the presence of LGS (0.17±0.03, 0.19±0.04, 0.17±0.03, 0.14±0.04, 0.11±0.02) compared to those in the absence of LGS (0.26±0.03, 0.23±0.05, 0.25±0.06, 0.27±0.10, 0.30±0.10). Similarly, the zeta potential kept more negative with LGS (-15.62±2.51, -13.03±2.94, -13.27±1.36, -16.00±1.86, -15.15±3.37) than without LGS (-4.37±3.00, -10.62±5.38, -3.44±2.27, -6.87±2.22, -5.47±2.02), supporting the efficacy of LGS in the formation of ethosomes and Tryp-ES. Therefore, the optimized formulation containing 30% propanediol, 10 mM DMPC and 0.03% LGS was prepared and used in the synthesis of ethosomes via the designed one-step microfluidic method.

Morphology of ethosomes by TEM and AFM

The external morphology of the optimized formulation of empty ethosomes or Tryp-ES with or without LGS was examined by TEM (Fig. 1A-D) and AFM (Fig. 1E-H), respectively. By TEM, the free ethosomes were found to have a predominantly spherical multilamellar structure with an average size of 154.60±38.42 nm, indicative of the successful formation of ethosomes through the tight arrangement of phospholipids (Fig. 1A and Fig. S1A) [33]. The addition of LGS resulted in a smooth, near-spherical structure with reduced surface tension and a particle size of 103.10±26.38 nm (Fig. 1B and Fig. S1B), which may enhance its dispersibility and deformability for topical penetration [24]. Once Tryp was loaded into the phospholipid bilayer structure, the obtained structures of nanovesicles appeared to be round or irregular (Fig. 1C and D). The prepared Tryp-ES without LGS had a smaller particle size of 77.56±17.91 nm (Fig. 1C and Fig. S1C), while the addition of LGS resulted in more irregularly shaped unilamellar vesicles with a larger particle size of 152.60±25.59 nm (Fig. 1D and Fig. S1D).

When examined by AFM, the geometric information on ethosomes could been further provided. The height of free ethosomes was 45.98±1.00 nm (Fig. 1E), while Tryp-loaded ethosomes had a height of 26.80±1.76 nm (Fig. 1G). The decreased height of Tryp-ES can be attributed to the surface-active properties of the drug molecule [34]. In the presence of LGS, the free ethosomes had a height of 12.44±1.38 nm (Fig. 1F), whereas Tryp-ES had a reduced height of 6.08±0.54 nm (Fig. 1H). Therefore, the incorporation of LGS in ethosomes helped to form smaller and more homogeneous nanoparticles, thereby contributing to skin permeability for efficient drug delivery [35]. The small unilamellar vesicles' spherical structure observed by AFM could be due to distinctive sample preparation methods and imaging environments as compared to TEM [36].
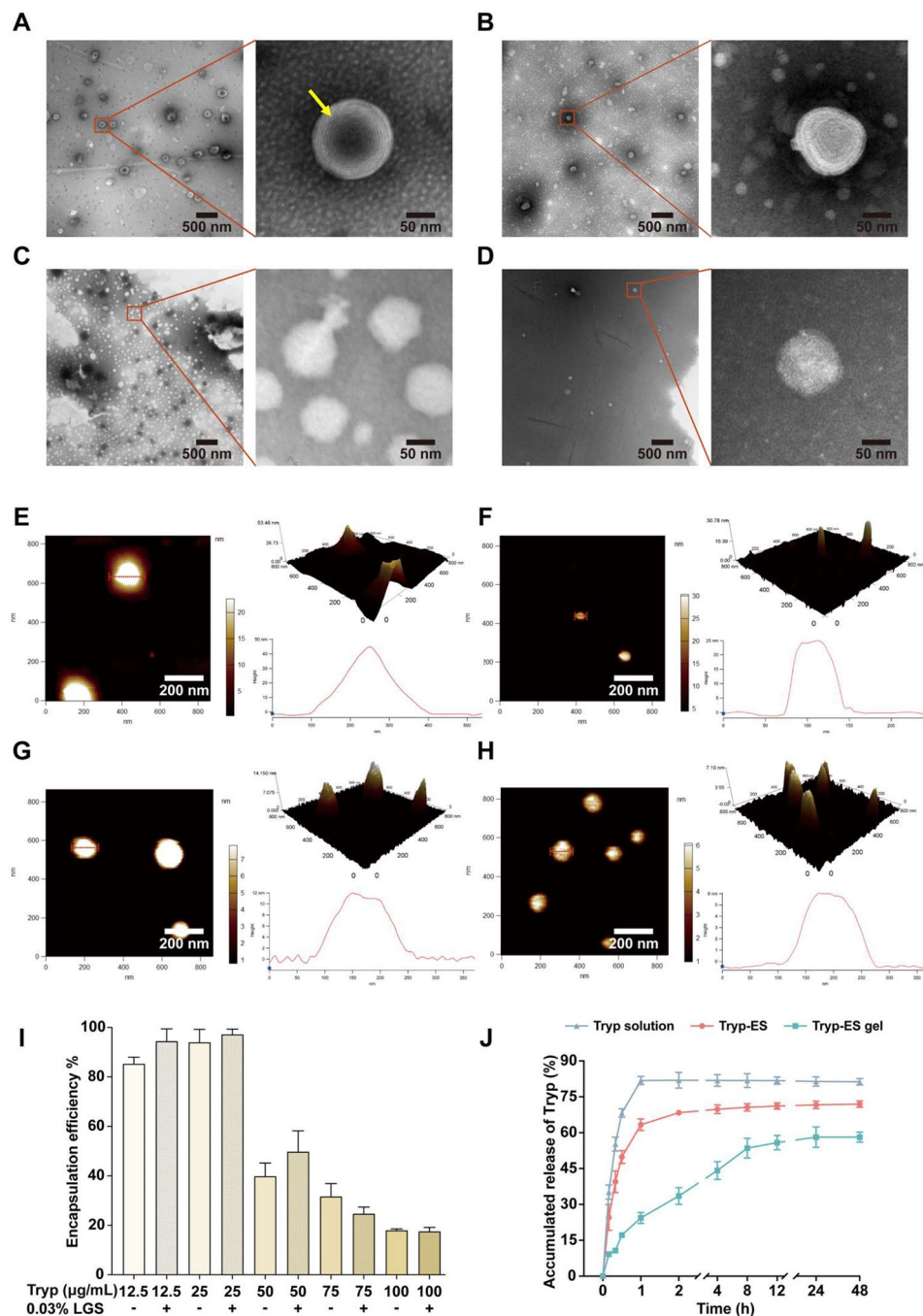
Wang *et al. Journal of Nanobiotechnology*   (2024) 22:584

Page 9 of 21

Fig. 1 Characterizations of Tryp-loaded ethosomes (Tryp-ES). (**A**-**D**) TEM images of empty ethosomes without LGS (**A**), empty ethosomes with 0.03% LGS (**B**), Tryp-ES without LGS (**C**), and Tryp-ES with 0.03% LGS (**D**). Yellow arrow represents the multiple lamellae of the empty ethosome. Scale bar: 500 nm (50 nm for magnified images). (**E**-**H**) AFM images for morphological and topographical analysis of empty ethosomes without LGS (**E**), empty ethosomes with 0.03% LGS (**F**), Tryp-ES without LGS (**G**), and Tryp-ES with 0.03% LGS (**H**). Scale bar: 200 nm. (**I**) The encapsulation efficiency of Tryp in ethosomes at different Tryp concentrations with or without 0.03% LGS. (**J**) Release profile of Tryp from Tryp solution, Tryp-ES and Tryp-ES gel for 48 h in 10% propanediol. Bars represent the mean ± SEM of 3 independent assays

Entrapment efficiency and in vitro drug release of Tryp-ES

Entrapment efficiency is a critical parameter for evaluating the quality of a drug delivery system, where the amount of encapsulated drug directly reflects its potential biological effects. Accordingly, the concentration

of Tryp was determined using a calibration curve (Fig. S2). Here, we determined the encapsulation rate of different concentrations of Tryp-loaded ethosomes and compared their entrapment efficiency in the presence or absence of LGS. As shown in Fig. 1I, 25 µg/ml Tryp

as initial drug input had the maximum entrapment efficiency of 97.19±2.95% among all formulations. However, when the Tryp input exceeded 25 µg/ml, the entrapment efficiency decreased dramatically, accompanied by drug precipitation, possibly due to drug overloading. Notably, consistent with the positive role of LGS in the uniformity and stability of ethosomes and Tryp-ES, the addition of LGS slightly improved the entrapment efficiency of Tryp-ES (Table 4), which may be attributed to the role of the surfactant in promoting a more ordered arrangement of lipid molecules, thereby enhancing the integrity of the lipid bilayer and reducing drug leakage [37]. Taken together, the optimal drug loading parameter for achieving the highest entrapment efficiency of Tryp-ES was 25 µg/ml Tryp in the presence of 0.03% (w/v) LGS.

Next, the release profile of Tryp from ethosomes (Tryp-ES) in comparison to Tryp solution and Tryp-ES gel was investigated in vitro at specified time points up to 48 h at 32±1 °C. As shown in Fig. 1J, all formulations exhibited a biphasic drug release profile. In particular, the Tryp solution rapidly achieved up to 82.15±1.72% of the total drug release within the first 1 h, followed by a stable plateau profile. In the case of Tryp-ES, a relatively slower and lower drug release was observed, reaching its plateau at 2 h (68.35±0.71%) and approximately 71.95±1.31% of Tryp being detected at 48 h. In contrast to the Tryp solution and Tryp-ES, only 33.52±3.49% of Tryp release was detected within the first 2 h with Tryp-ES gel, which showed a linear increase until 12 h, with 58.15±2.11% at the end of 48 h. Due to the potential for skin irritation from high propanediol concentrations and rapid drug release [38], as well as the hygroscopic nature of propanediol in the drug solution, which may result in drug precipitation in the presence of excessive water, the propanediol solution of Tryp is unsuitable for practical application. Moreover, the dual release pattern of Tryp-ES can be attributed to the "penetration enhancer" effect of propanediol [39]. The incorporation of propanediol into ethosomal systems endows them with enhanced flexibility and facile diffusion across membranes. However, this also results in a reduction of the hydration layer surrounding the vesicles and a disruption of the structural integrity of the lipid bilayers, thereby facilitating the first phase of drug release from Tryp-ES [37]. As solvent diffusion and drug concentration decreased over time, the lipid bilayers may have partially regained order and integrity, thereby gradually slowing the rate of drug release. Furthermore, the in vitro drug release profile of Tryp-ES gel also showed a dual release pattern, consistent with the principles of drug diffusion and/or hydrogel degradation, as previously reported [40, 41]. It is noteworthy that the incorporation of Tryp-ES into a gel system resulted in a limited dissolution of Tryp, with 33.52±3.49% at 2 h and 58.15±2.11% at 48 h, respectively. The reduced rates were mainly attributed to the obstructive effect of the gel structure, which impedes diffusion.

Stability assessment of Tryp-ES

Different storage conditions may have substantial impacts on the physical and chemical stability of ethosomes, leading to the alteration in particle size, PdI, zeta potential, and drug encapsulation efficiency. This can result in a loss of their expected biological responses. To investigate the influence of storage conditions on Tryp-ES stability, collected samples were stored at 4–25 °C for upto 28 days, respectively. At the end of the indicated storage periods, the particle size of Tryp-ES gradually increased from 97.37±3.95 nm to 106.80±6.03 nm at 4 °C, and from 98.25±3.79 nm to 107.70±3.26 nm at 25 °C (Fig. 2A). No changes were found in PdI when samples were stored at both 4 °C and 25 °C (Fig. 2B). Zeta potential exhibited a gradual decrease from -17.68±0.11 mV to -16.50±0.55 mV at 4 °C, and from -17.72±0.09 mV to -15.87±0.17 mV at 25 °C (Fig. 2C). Moreover, as shown in Fig. 2D, stability tests revealed that Tryp-ES was more stable at 25 °C, where approximately 80.46±1.08% of Tryp remained after 28 days. In contrast, only 33.95±3.88% of Tryp remained after 28 days at 4 °C. These results collectively suggest that Tryp-ES maintained its physicochemical characteristics well over a storage of 28 days at RT (25 °C), compared to those at 4 °C. However, the stability of Tryp-ES could be affected by a number of factors, including temperature, the nature of the solvent propanediol, the chemical stability of Tryp itself, and the composition and structure of the ethosome. In particular, the physical properties of the solvent propanediol, such as viscosity, vary with temperature. At RT, propanediol-derived ethosomes are more fluid, which generally helps to keep Tryp encapsulated within the ethosome, whereas at lower temperatures, propanediol becomes more viscous, which may contribute to reduced solubility of Tryp encapsulated in Tryp-ES, leading to promoted leakage of Tryp. Our result revealed that 4 °C was indeed less favorable for stability than RT, particularly in terms of encapsulation efficacy, strongly suggesting that RT is more appropriate for the viscosity of propanediol, which may provide a more stable environment with less Tryp leakage from Tryp-ES. Meanwhile, the Tryp-ES gel was characterized for its physical appearance, pH and drug content over 28 days at 4 °C and 25 °C, respectively (Fig. S3). The results showed that these Tryp-ES were more stably incorporated into this semi-solid formulation.

Cellular uptake, cell proliferation and cell apoptosis in vitro

Before evaluating the bioactivity of Tryp-ES on cells, we first determined its cytotoxicity in HaCat cells. As shown in Fig. S4A, incubation of HaCat cells with 300
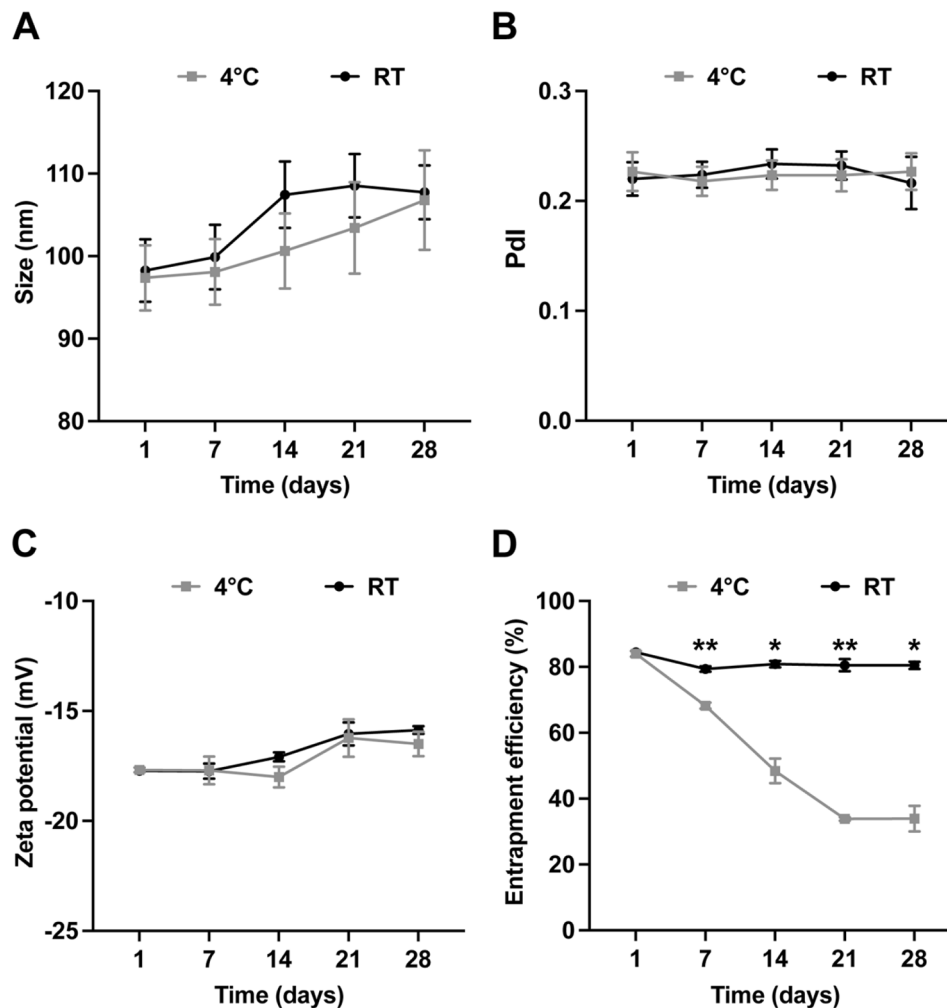
Fig. 2 Stability assessment of Tryp-ES. (**A**-**D**) Changes in particle size (**A**), size distribution (PdI, **B**), zeta potential (**C**), and entrapment efficiency (**D**) of Tryp from Tryp-ES over 28 days storage at 4 °C and 25 °C (RT). Bars represent the mean ± SEM of 3 independent assays. $^*p < 0.05$, and $^{**}p < 0.01$ compared with RT

ng/ml Tryp-ES for 48 h did not significantly affect HaCat cell viability. Since the efficacy and cytotoxicity of drugs depend on their ability to enter and accumulate within cells, we used confocal fluorescence microscopy to examine the cellular uptake of Tryp-ES by HaCat. As shown in Fig. 3A, over an incubation period of up to 24 h, it was observed that Tryp was initially internalized by cells after 6 h incubation and accumulated in the cytoplasm from 12 h, which increased aggregation at 24 h. However, 300 ng/ml Tryp-ES was observed to be initially internalized by cells after 1–3 h of incubation, with the red autofluorescence of Tryp aggregating at the periphery of the cell membrane. After 6 h of exposure, Tryp could be observed in the cytoplasm of HaCat, and with increasing incubation time, intracellular Tryp accumulated dramatically at 12 h. 3D analysis of confocal microscopy images further confirmed the Tryp trans-localization into the cell nuclei at 24 h (Fig. 3B). As a negative control, empty ethosomes

didn't show any red fluorescence (Fig. S5A). These results indicate that Tryp-ES is able to efficiently enter HaCat cells, from the initial contact with the cell membrane to the final accumulation in the cell nucleus.

The colocalization of Tryp with the nucleus indicated that this drug might have potential effects on the hyper-proliferation of cells as seen in psoriasis. To test this possibility, we used EGF or KGF at 20 ng/mL as positive controls that induced cell proliferation (Fig. S5B) and found that both Tryp solution and Tryp-ES inhibited the proliferation of cells induced by EGF and KGF in a dose-dependent manner (Fig. 3C). Specifically, Tryp-ES suppressed KGF-induced cell growth by up to 41.3%, whereas Tryp solution inhibited cell growth by up to 8.7%. Moreover, Tryp-ES inhibited EGF-promoted cell growth by 31.1% and Tryp solution inhibited it by 11.5%. The inhibitory effects varied between Tryp solution and Tryp-ES as the dose increased, in which Tryp-ES
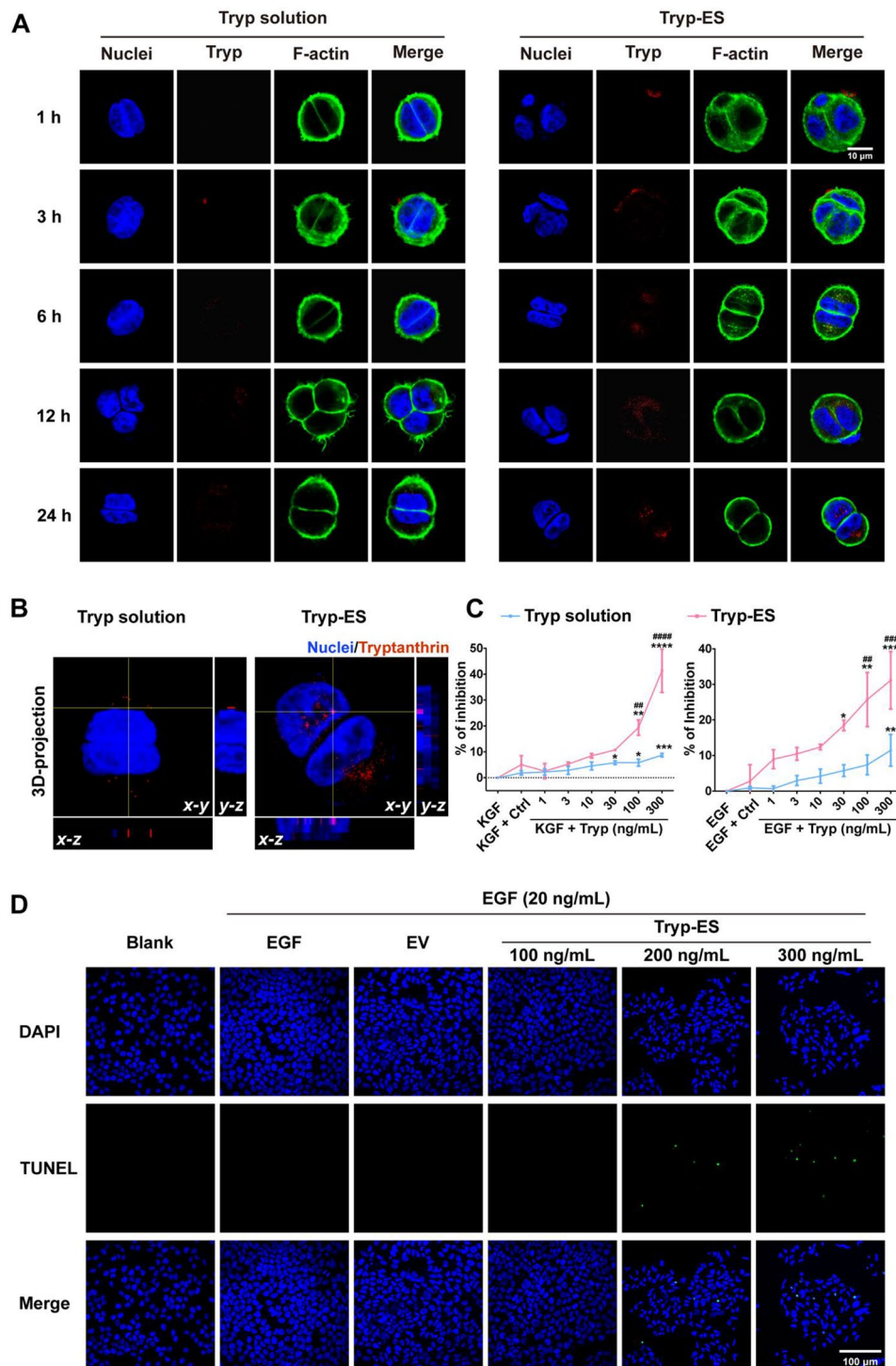
Fig. 3 Effects of Tryp-ES on cell proliferation and apoptosis in vitro. (**A**) Cellular uptake of Tryp solution or Tryp-ES for the indicated time points (blue, nuclei; red, Tryp; green, F-actin). Scale bar: 10 µm. (**B**) Representative three-dimensional images of cells, including a top-down view in the X-Y plane and longitudinal cross-sectional views in the X-Z and Y-Z planes to examine the internalization of Tryp after incubation with Tryp solution or Tryp-ES for 24 h (blue, nuclei; red, Tryp). (**C**) Inhibitory effects of Tryp solution or Tryp-ES on KGF (20 ng/mL) or EGF (20 ng/mL) induced cell proliferation. Data are presented as the mean ± SEM ($n = 3$). $^{*}p < 0.05$, $^{**}p < 0.01$ and $^{***}p < 0.005$ compared with KGF or EGF; and $^{\#\#}p < 0.01$, $^{\#\#\#}p < 0.001$, and $^{\#\#\#\#}p < 0.0001$ compared with Tryp solution. (**D**) Micrographs of TUNEL-positive (green) expression of apoptotic cells in EGF-induced HaCat cells indicated with Tryp-ES for 24 h (green, TUNEL; blue, nuclei). Scale bar: 100 µm

demonstrated more promising inhibitory capacity than Tryp solution. To further explain the reason why Tryp-ES dramatically suppressed cell proliferation, we assessed cell apoptosis, which is the main strategy to control excessive cell proliferation. Using TUNEL assays, which are subjected to extensive DNA degradation during the late of apoptosis [42], the amount of TUNEL-positive cells increased in dose-dependent manner after 24 h of Tryp-ES exposure compared to HaCat cells treated with EGF alone (Fig. 3D) and Tryp solution (Fig. S5C). Taken together, these results suggest that Tryp-ES can potentially inhibit the excessive proliferation of keratinocytes by inducing apoptosis, making it a viable therapeutic agent for the treatment of psoriasis.

In vitro inhibition of angiogenesis by Tryp-ES

Abnormal blood vessel growth in psoriatic lesions usually causes erythema and bleeding [3, 43], and therefore, one of the therapeutic strategies for psoriasis is targeting angiogenesis [44]. Our previous studies have confirmed the anti-angiogenic properties of Tryp at concentrations ranging from 3 to 100 μM (0.75–25 μg/mL) [31], we accordingly focused on the effects of Tryp-ES on angiogenesis. Based on the safety profiles of Tryp-ES (37.5–300 ng/mL) on HUVEC (Fig. S4B), tube formation analysis was performed in the presence of 50 ng/mL bFGF, which induced a massive network of well-branched tubes (Fig. 4A, bFGF). Even though the concentration of Tryp significantly decreased, a dose-dependent disruption of tube formation was observed in HUVEC treated with Tryp-ES, as evidenced by the suppression of vessel density, total number of junctions, and total tube length (Fig. 4A-B). These results suggested that Tryp-ES may exert therapeutic potential in psoriasis by inhibiting angiogenesis.

In vitro skin permeation and retention of Tryp-ES

Efficient skin permeation and retention are essential for topical drug administration. For Tryp-ES, to carry out its biological activities, it requires Tryp to successfully permeate through scaly psoriasis lesions and retain in the epidermis and deeper dermis. Given that hydrogel-based products have been used as an effective topical drug delivery system for cutaneous conditions due to their hydration and bioadhesiveness properties [45, 46], we developed and employed ethosomes gel, in comparison with ethosomes, for their skin penetration efficiency. To determine whether ethosomes in the form of gel are more effective in drug penetration, we employed psoriatic mice treated with Rhodamine B-loaded ethosomes (RhB-ES) or RhB-ES gel. As shown in Fig. 5A, after the initial 10 min of application, red fluorescence of RhB was observed within the SC layer and upper epidermis of the mice skin for both RhB-ES and RhB-ES gel. With

continued administration for 20 min, 30 min and 60 min, enhanced delivery of RhB in terms of depth (viable epidermis, hair follicle, dermis) was observed in the skin treated by RhB-ES (Fig. 5A, upper panels). On the contrary, the penetration of RhB from RhB-ES gel was limited to the upper layer of the mice skin (Fig. 5A, lower panels). This set of data suggested that RhB-ES was more favorable for drug penetration within a short period of time, while RhB-ES gel only enabled a slow and sustained drug release, leading to long-term deposition in the epidermal layer.

Next, the capability of Tryp to retain and permeate in psoriatic skin was quantitatively compared between Tryp-ES and Tryp-ES gel using the Franz diffusion cell, with the corresponding results illustrated in Fig. 5B-C. Before the test, we confirmed 0.25% trypsin-EDTA incubated at 37 °C for 2 h resulted in the successful separation of dermis and epidermis (Fig. S6, Table S1). As shown in Fig. 5B, the skin retention of Tryp in the epidermis and dermis of Tryp-ES (133.20 ± 16.43 ng/cm^2 and 121.20 ± 5.07 ng/cm^2, respectively) was higher than those of Tryp solution (96.87 ± 5.96 ng/cm^2 and 96.16 ± 6.41 ng/cm^2, respectively), those of Tryp-ES gel (57.43 ± 6.79 ng/cm^2 and 53.10 ± 5.52 ng/cm^2, respectively), and those of Tryp gel (55.74 ± 3.37 ng/cm^2 and 34.73 ± 3.91 ng/cm^2, respectively). As 30% propanediol can potentially cause skin irritation, including skin defatting and barrier disruption [38], it is not suitable for practical application when used with Tryp. A similar trend was observed for skin permeation of Tryp, with the fastest and highest permeation of Tryp being achieved with Tryp-ES (Fig. 5C). In particular, skin permeation of Tryp was detected 30 min after exposure to Tryp-ES ($1.43 \pm 0.22\%$) and Tryp solution ($0.73 \pm 0.21\%$), 40 min after application of Tryp-ES gel, and 50 min after application of Tryp gel. Overall, Tryp-ES exhibited higher skin retention and permeation of loaded drugs compared to Tryp solution, Tryp-ES gel and Tryp gel during the 1 h topical administration. Considering daily topical application, multiple time points at 1, 2, 4, 8, 24 h were selected to evaluate drug retention and permeation. Although the retention of Tryp in both epidermis and dermis from Tryp-ES and Tryp-ES gel decreased over 24 h, the retention of Tryp was higher with Tryp-ES than with Tryp-ES gel at each time point, reaching the minimum amount at 24 h (Fig. S7A). Meanwhile, the permeation of Tryp from Tryp-ES and Tryp-ES gel gradually increased over 24 h, reaching a maximum of $32.12 \pm 1.19\%$ and $16.24 \pm 1.35\%$ at 24 h, respectively (Fig. S7B).

To further understand why Tryp encapsulated in ethosomes is more capable of penetrating psoriatic lesions, we investigated the effects of ethosomes on the integrity of cell membranes, using in situ Cypher ES AFM imaging of DMPC/DMPG-prepared bilayers supported on mica
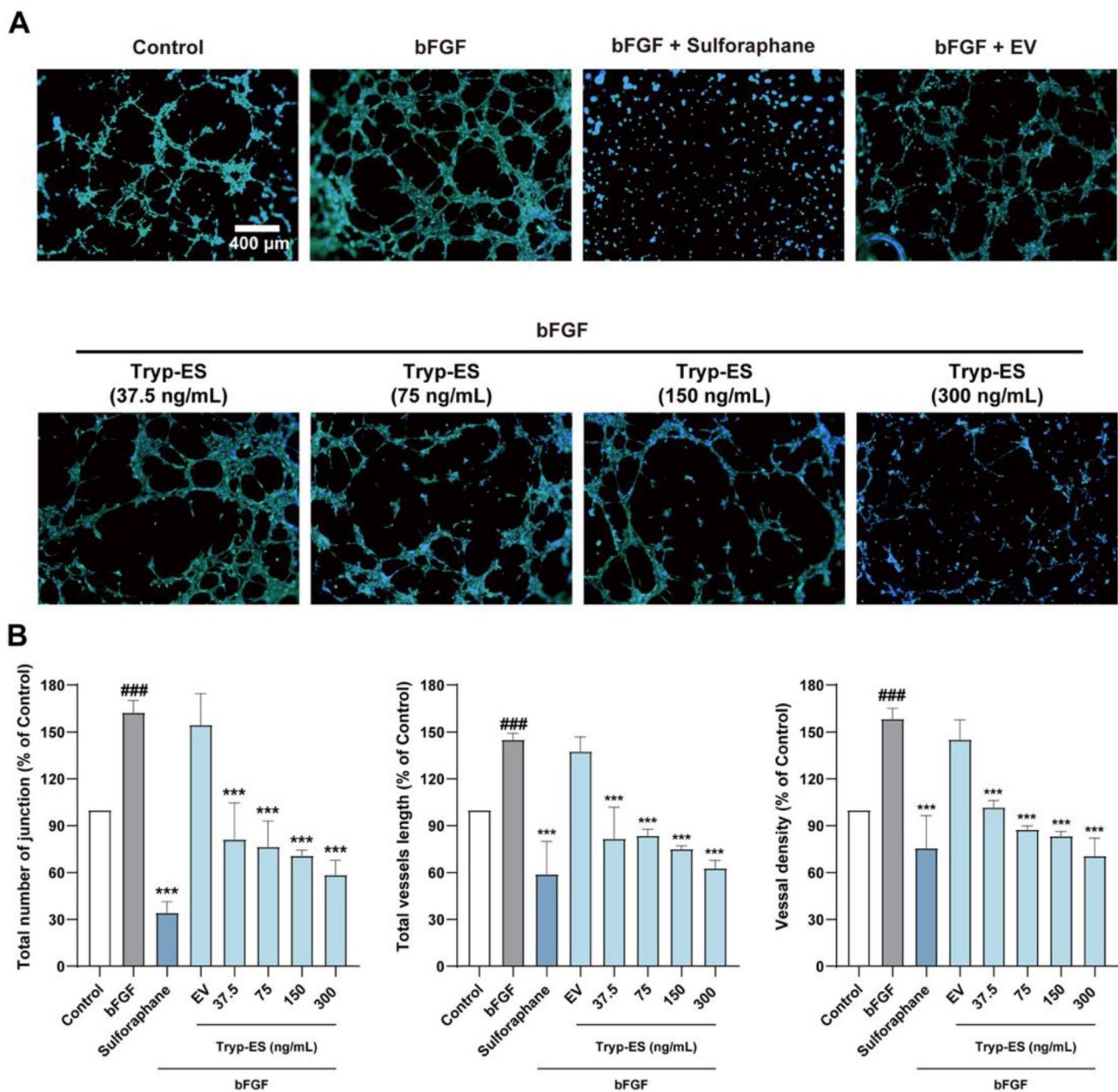
Fig. 4 Effects of Tryp-ES on bFGF-induced HUVEC tube formation in vitro. (**A**) Representative images of bFGF-induced HUVEC tube formation with the indicated Tryp-ES (37.5 ng/mL, 75 ng/mL, 150 ng/mL and 300 ng/mL) in comparison with positive control sulforaphane. Scale bar: 400 μm. (**B**) Quantitative analysis of each treatment by calculating vessel density (percentage of area covered by vessels), total number of junctions, and total vessel length from the obtained images using NIH Image J. Data were normalized to the control group (mean ± SEM, $n = 3$; $^{###}p < 0.005$ compared with control; $^{***}p < 0.005$ compared with bFGF)

substrates. The impact of ethosomes on the structure of the bilayer membrane was recorded in real-time (Fig. 5D). Following the addition through injection of ethosomes into AFM liquid chamber, newly formed pores or defects in the lipid bilayer were captured. Gradually, an expansion of the preexisting defects occurred. Intriguingly, after 30 min, these expanded pores or enlarged holes tended to shrink and returned to their initial state over 120 min. Hence, the lipid bilayer membrane undergoes a

process from transient destruction to a subsequent restoration in response to ethosomes exposure. Although successful real-time imaging with Tryp-ES was achieved, it is not possible to perform in situ imaging of Tryp-ES in gel using AFM due to the semi-solid state of the gel, which severely affects AFM scanning. Our results showed that ethosomes directly disrupted the bilayer membrane for drug delivery, which was subsequently restored 30 min after ethosomes exposure. The reduced drug retention
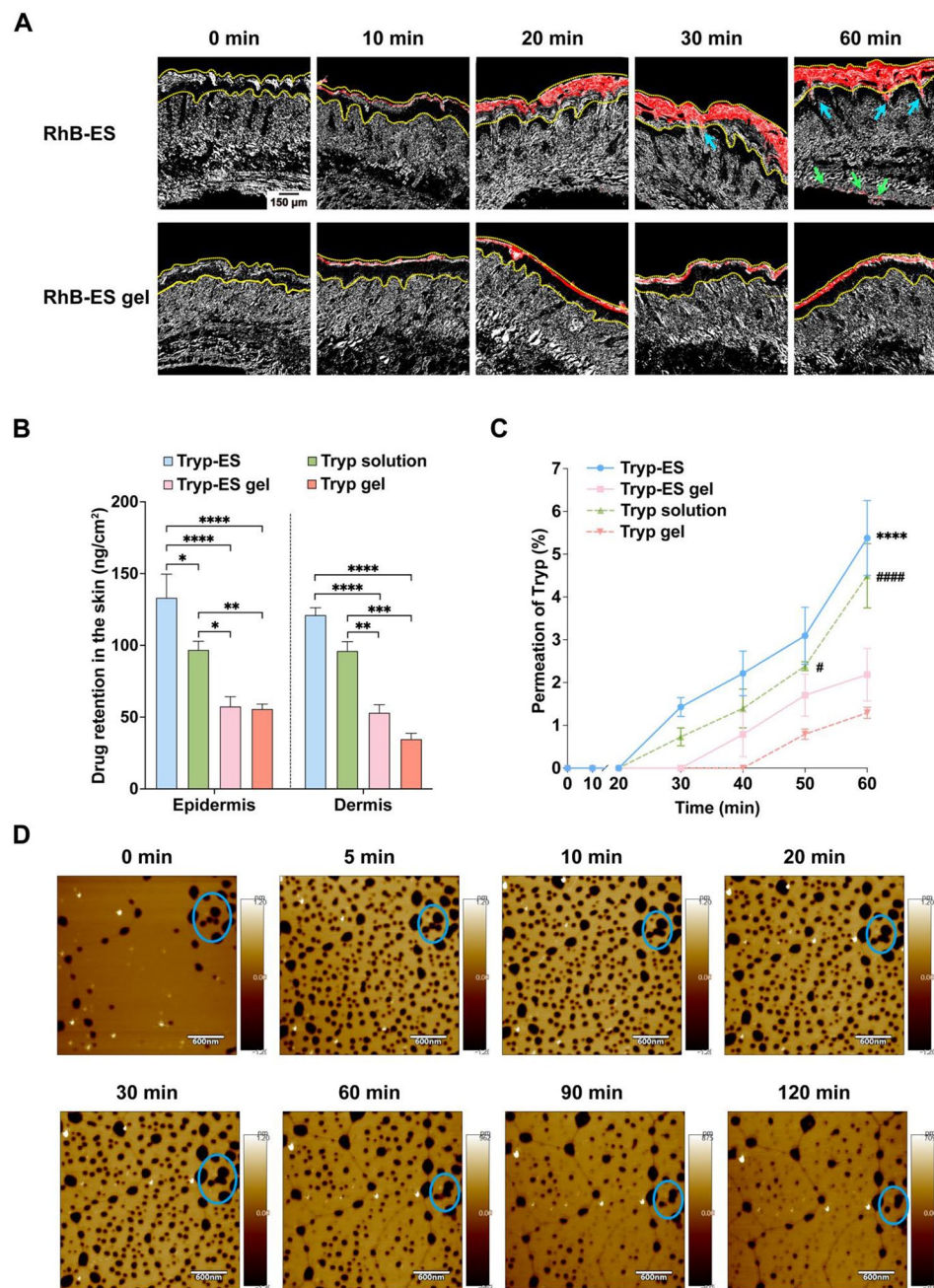
Fig. 5 Topical permeation of drugs by ethosomes. (**A**) Representative confocal laser scanning images of IMQ-induced psoriatic mice skin exposed to Rhodamine B-loaded ethosomes (RhB-ES) or RhB-ES gel at 0, 10, 20, 30 and 60 min after topical administration (Red, rhodamine B fluorescence; dashed yellow lines: indicate the epidermis; blue arrow: hair follicle; green arrow: deep dermis). Scale bar: 150 μm. (**B**) The retention of Tryp in the epidermal and dermal layers of psoriatic mice skin was determined by HPLC after 60 min treatment with Tryp-ES, Tryp-ES gel, Tryp solution or Tryp gel using Franz diffusion cells. Data are presented as the mean ± SEM ($n = 3$), $^*p < 0.05$, $^{**}p < 0.01$, $^{***}p < 0.001$ and $^{****}p < 0.0001$ as indicated. (**C**) The permeation of Tryp was examined at different time points during the 60 min treatment with Tryp-ES, Tryp-ES gel, Tryp solution or Tryp gel using Franz diffusion cells. Data are presented as the mean ± SEM ($n = 3$), $^{****}p < 0.0001$ vs. Tryp-ES gel; $^#p < 0.05$, and $^{####}p < 0.0001$ vs. Tryp gel. (**D**) The sequential surface changes of supported DMPC/DMPG (4:1) lipid bilayers. AFM images were obtained in real-time before (0) and after the injection of ethosomes at 5, 10, 20, 30, 60, 90 and 120 min. The blue circle shows the region where the surface of DMPC/DMPG bilayer has been altered by ethosomes. Scale bar: 600 nm

and permeation observed in the Tryp-ES gel compared to the Tryp-ES during the 1 h topical administration period may be attributed to the restriction of mobility and flexibility of the ethosomes by the gel matrix, which impedes

the penetration of the drug through the skin barrier. This finding is consistent with previous observations that the viscous structure of the gel dramatically inhibits drug diffusion [47]. The high fluidity and deformability of

ethosomes facilitate their penetration through skin pores [48], rendering then more favorable for drug penetration and retention compared to their gel counterpart.

Amelioration of psoriatic phenotypes by Tryp-ES in IMQ-induced mice

To evaluate the anti-psoriatic efficacy of Tryp-ES and Tryp-ES gel in vivo, different dosing frequencies of free ethosomes (EV_1: single dose, EV_2: double dose, EV_3: triple dose), Tryp-ES (Tryp-ES_1: single dose, Tryp-ES_2: double dose, Tryp-ES_3: triple dose), and their corresponding formulation in gel were applied topically for 1 h per day to the shaved back skin of BALB/c mice subjected to IMQ cream for 7 consecutive days (Fig. 6A). CP ointment treatment was used as a positive control. For all groups, the weight and psoriasis area of each mouse were monitored daily, and all mice were assessed for the severity index (PASI) score by evaluating the degree of erythema and scaling. A macroscopic examination showed that mice treated with IMQ displayed expected symptoms such as weight loss and psoriatic inflammation along with a significantly higher PASI score in comparison to healthy mice (Fig. 6B-C). When compared to IMQ-induced model, all treatments showed an overall reduction in skin erythema and scaling at day 7. The mice treated with triple dosing of Tryp-ES (Tryp-ES_3) showed the most noticeable ameliorations of psoriatic lesions especially in scaling and erythema score, as compared to IMQ-treated model. Interestingly, more frequent dosing of free ethosomes also decreased the severity of erythema and scaling of skin lesions, which indicated the potential therapeutic efficacy of lipid-based nanoparticles. In addition, a similar trend of recovery was observed with the gel formulation of free ethosomes and Tryp-ES. This could be attributed to the hydrating effect of the gel, which moisturizes the SC and seals the skin, thereby reducing transepidermal water loss (TEWL). This is advantageous for the restoration of scaling, dryness, and disruption of the skin barrier in psoriatic lesions [49]. Nevertheless, the therapeutic efficacy of gel formulations was found to be inferior to that of their liquid counterparts. This is likely attributable to the viscous structure of the gel, which impedes the diffusion of drug [47].

Pathological analyses of IMQ-induced psoriatic mice

To comprehensively understand the therapeutic effects of Tryp-ES, histopathological evaluations were performed with the treated skin from all groups of mice (Fig. 7A and B). By analyzing H&E staining, we verified the finding that all ethosomes-exposed groups have an inhibitory effect on epidermal parakeratosis and hyperkeratosis compared to IMQ-treated model, among which the triple-dose of Tryp-ES (Tryp-ES_3) had the most favorable results. To better characterize the effect of Tryp-ES on epidermal hyperplasia, hyperproliferating keratinocytes stained with Ki67$^+$ were analyzed. The results demonstrated that Tryp-ES reduced the number of Ki67$^+$ cells in a dose-dependent manner, with $-39.68\pm0.66\%$ in Tryp-ES1 (EV1: $-35.80\pm7.55\%$), $-47.88\pm3.38\%$ in Tryp-ES2 (EV2: $-38.10\pm4.15\%$), and $-62.08\pm9.09\%$ in Tryp-ES3 (EV3: $-51.85\pm2.04\%$) compared to the IMQ-induced untreated model. Additionally, all treated groups demonstrated a prevention of psoriatic phenotypes on erythema, which includes T cells infiltration, neoangiogenesis, and vascularity. Accordingly, CD3$^+$-stained infiltrating T cells and CD31$^+$-stained angiogenesis cells were analyzed. Among all treated groups, mice treated with Tryp-ES_3 led to the most significant reduction in the mean population of CD3$^+$ cells ($-74.52\pm5.32\%$ *vs.* EV_3: $-63.34\pm5.60\%$) and CD31$^+$ cells ($-45.65\pm3.40\%$ *vs.* EV_3: $-19.37\pm1.38\%$), indicating that more frequent Tryp-ES administration represents more effective outcomes (Fig. 7B). However, triple-dosing did not significantly improve the therapeutic effect compared to double-dosing, suggesting that the dosing more than three is not necessary. When compared the two different formulations of Tryp-ES in liquids and gels, ethosomes in liquids consistently exhibited the more remarkable reduction in the mean population of Ki67$^+$ cells, CD3$^+$ cells and CD31$^+$ cells. These results were in line with the ex vivo data demonstrating that ethosomes could exert a better anti-psoriasis effect than their gel counterpart by permeating to deeper layers of psoriatic skin.

Meanwhile, the safety profile of Tryp-ES was confirmed through pathological studies of the liver, kidney, and spleen (Fig. S8A). The results showed that neither the control nor the treatment groups exhibited any obvious organ damage, supporting that Tryp-ES did not exhibit significant histopathological toxicity in vivo. Moreover, biochemical parameters of blood serum were also measured, and no differences were found in the levels of ALT, AST, TP, ALB, GLB, LDH, CK, BUN, and CR among all the groups except for the positive control CP, which induced a significant increase in ALT and GLB levels, probably resulted in potential side effect of liver dysfunctions (Fig. S8B).

Collectively, the histopathological study confirmed the therapeutic efficacy of Tryp-ES in the IMQ-induced psoriatic models. Therefore, taking advantage of ethosomes in assisting drug delivery, Tryp obtains the better chance to reach deeper lesions of psoriatic skin to exert anti-proliferative, anti-inflammatory, and anti-angiogenic activities, resulting in improved therapeutic outcomes. Notably, during all these evaluations, we also noticed a direct anti-psoriatic effect of free ethosomes, such as in the control of CD3$^+$ cells (Fig. 7B), suggesting that the phospholipid composition of ethosomes may additionally
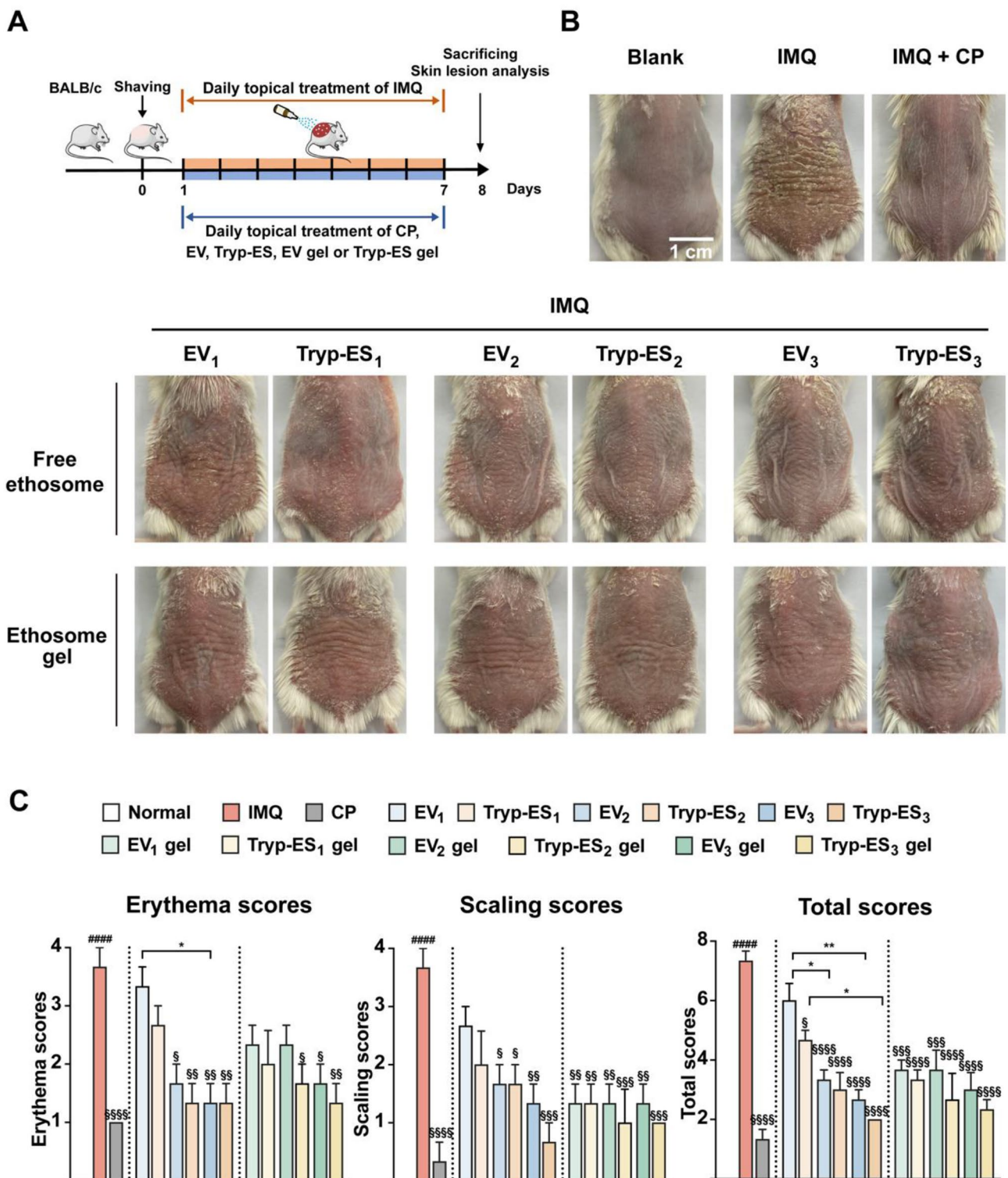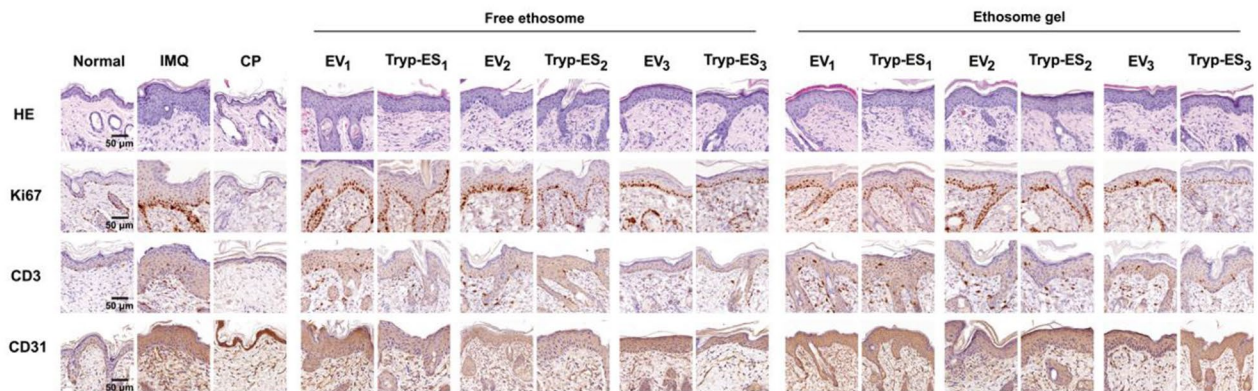
Fig. 6 Amelioration of psoriatic phenotypes by Tryp-ES or Tryp-ES gel in IMQ-induced mice. (**A**) Experimental design for evaluating the anti-psoriasis efficacy of Tryp-ES or Tryp-ES gel in IMQ-induced psoriatic mice. (**B**) The macroscopic appearance of dorsal shaved skin of mice at day 7 following treatment with indicated formulations. Ethosome vehicle: EV_1 (single dose), EV_2 (double dose), EV_3 (triple dose); Tryp-ES: Tryp-ES_1 (single dose), Tryp-ES_2 (double dose), Tryp-ES_3 (triple dose). Each dose of EV contained 1 µM DMPC, Tryp-ES contained 1 µM DMPC and 1.5 µg Tryp. Scale bar: 1 cm. (**C**) Assessment includes erythema, scaling, and total PASI scores of IMQ-induced psoriatic dorsal skin treated with indicated formulations ($n = 3$). Data are presented as the mean ± SEM. $^{####}p < 0.0001$ *vs*. Normal control without any drug treatment; $^{§}p < 0.05$, $^{§§}p < 0.01$, $^{§§§}p < 0.001$ and $^{§§§§}p < 0.0001$ *vs*. IMQ; $^{*}p < 0.05$ and $^{**}p < 0.01$ between treatments as indicated

Wang *et al. Journal of Nanobiotechnology*   (2024) 22:584
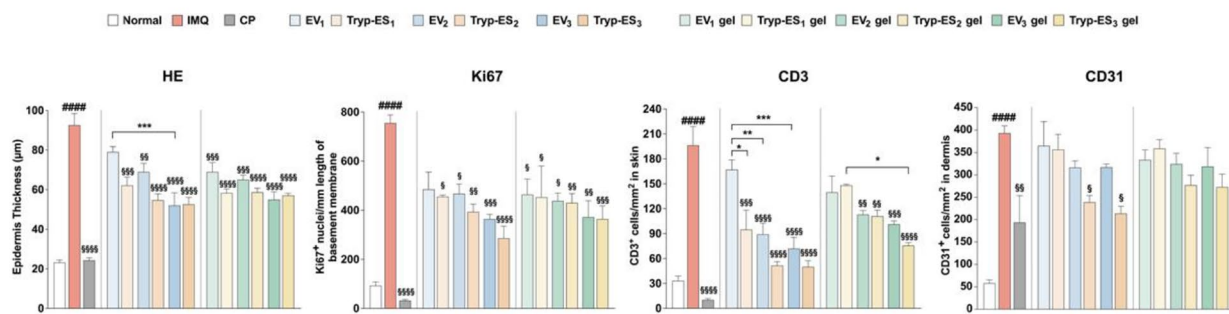
Page 18 of 21

Fig. 7 Histopathological examinations of dorsal skin in response to Tryp-ES or Tryp-ES gel in IMQ-induced psoriatic mice. (**A**) H&E staining, the expression of Ki67^{+}, CD3^{+}, and CD31^{+} of the dorsal skin of psoriatic mice treated with indicated formulations. Scale bar: 50 μm. (**B**) Quantifications of epidermal thickness, Ki67^{+}-positive cells, CD3^{+}-positive cells, and CD31^{+}-labelled cells ($n = 3$). Data are presented as the mean ± SEM. [####]$p < 0.0001$ *vs.* Normal control without any drug treatment; [§]$p < 0.05$, [§§]$p < 0.01$, [§§§]$p < 0.001$ and [§§§§]$p < 0.0001$ *vs.* IMQ; [**]$p < 0.01$, [***]$p < 0.001$ and [****]$p < 0.0001$ between treatments as indicated

function as complementary therapeutic agents to alleviate psoriasis-like dermatitis [17].

Lipidomic analyses in IMQ-induced psoriatic mice

Considering the lipid disorders in the pathogenesis of psoriasis [50, 51] and the observed therapeutic effect of ethosomes on psoriatic skin, we performed a lipidomic analysis of experimental skin samples to investigate the potential regulatory effects of ethosomes on lipid metabolism in IMQ-induced psoriatic skin lesions. For this analysis, freshly isolated dorsal skin samples were collected and subjected to lipid profiling by LC-MS analysis. Principal component analysis (PCA) showed a good overall separation among groups of Normal, IMQ, and ethosomes/Tryp-ES based on their lipid profiles (Fig. 8A). A similar clustering trend of ethosomes and Tryp-ES was observed, and these two groups were scattered in the area between the Normal and IMQ groups along the PC1/PC2 score plot (Fig. 8A). We next performed a univariate analysis with all the lipids found between IMQ and other groups, respectively. Volcano plots were constructed to visualize the distribution of differentially expressed lipid metabolites (DELs) among lipids species

with the positive or negative fold change between two groups applying fold change (FC) > 1.5 or < 0.67, variable important in projection (VIP) > 1, and $p < 0.05$ (Fig. 8B and D). We found phospholipid molecules, especially those belonging to the subclass of ceramides (Cer), hexosylceramide (Hex1Cer), phosphatidylcholines (PC), phosphatidylethanolamine (PE), triglycerides (TG), wax esters (WE), had varying degrees of changes in IMQ *vs.* control. Specifically, in IMQ-treated skin, the great majority of these altered phospholipids belonging to TG were increased, while those in Cer and WE were decreased (Fig. 8B). This is consistent with previous studies showing that patients with psoriasis are often accompanied by elevated TG [52], and that TG increases significantly in the skin lesions of IMQ-induced psoriatic mice [17]. Ceramides and wax esters play a crucial role in maintaining the skin barrier function [53–55]. The reduced levels of lipids could contribute to impaired skin barrier function in psoriatic mice. When compare ethosomes or Tryp-ES to IMQ models, ethosomes and Tryp-ES-treated groups partially restored the lipid alterations induced by IMQ in a similar pattern (Fig. 8C-D).
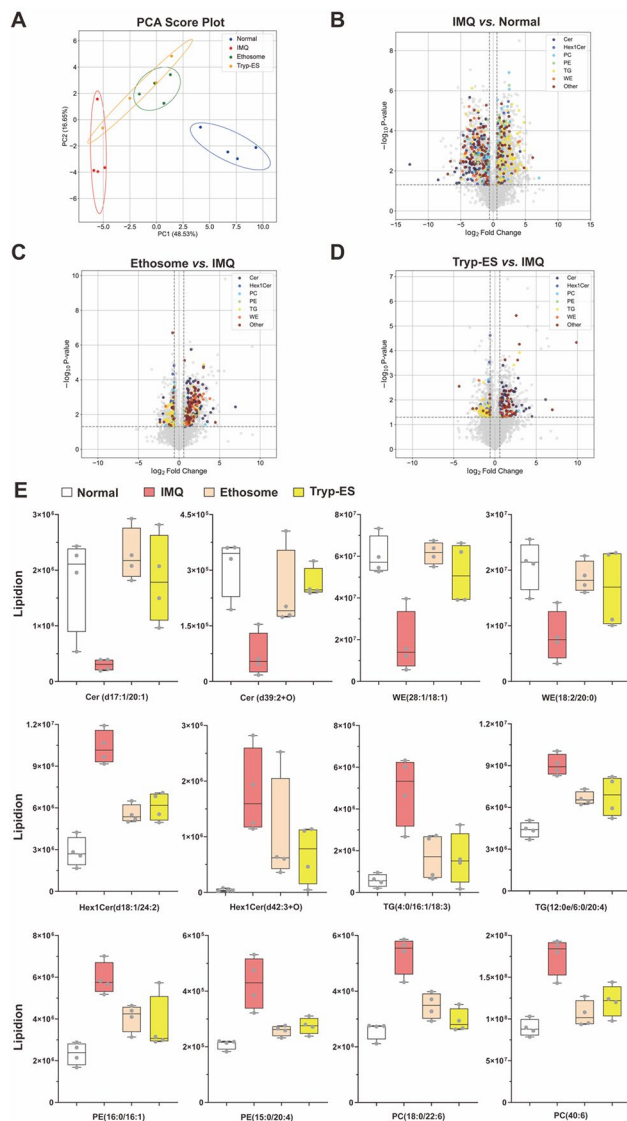
Fig. 8 Lipidomics analysis of skin lesions in IMQ-induced psoriatic mice with different treatments. (**A**) Principal component analysis (PCA) of lipidomics data. 16 samples were categorized into 4 clusters, each within the confidence ellipse corresponding to Normal control, IMQ, Ethosome, and Tryp-ES groups ($n = 4$). (**B**-**D**) Volcano plots of differentially expressed lipid metabolites (DELs) in the comparison of IMQ *vs.* Normal (**B**), Ethosome *vs.* IMQ (**C**), and Tryp-ES *vs.* IMQ (**D**), respectively. Each lipid subclass was marked with a unique color for distinction. (The selection criteria for differential molecules were fold change (FC) > 1.5 or < 0.67, VIP > 1, and $p < 0.05$.) (**E**) Changes of lipid metabolites level in psoriatic mice skin with different interventions ($n = 4$)

As depicted in Fig. 8E, the expression of the top 12 metabolites with the most significant differences from the above 6 subclasses was selected. These lipid molecules influenced by IMQ were all found to be restored by both ethosomes and Tryp-ES. Most of these DELs were present in distinct lipid species that exhibited long-chain and varying degrees of unsaturated fatty acid features. This variability may account for specific biological effects associated with psoriasis. For instance, very long-chain ceramides (long chain, ≥ C22) have been reported to have more protective effects [56] and exert apoptotic effects depending on their saturation degree [57]. More importantly, since the PC, PE and TG elevated in the skin tissues treated with IMQ were indispensable elements in constructing cell membranes, the boosting of these lipids could be associated with a rapid cell proliferation and division required for psoriasis, which may subsequently trigger the biosynthesis of phospholipids [51]. Taken together, our findings highlight the anti-psoriatic effect of ethosomes, which is mainly linked to anti-proliferation properties of lipid molecules and their abilities to improve the skin barrier function.

Conclusions

By precisely controlling the flow rate using a microfluidic device, we successfully prepared ethosomes and Tryp-ES, and further developed their gel formulations. Tryp-ES exhibited homogeneous particle size and favorable stability at RT. The fluidic properties of ethosomes facilitated themselves to penetrate across epidermal cells and even approach to the deep layers of the skin, thereby improving the delivery of the poorly soluble Tryp for more efficacious therapeutic outcomes within skin tissues. In cellular experiments, Tryp-ES exhibited notable efficacy in inhibiting angiogenesis and promoting apoptosis in abnormally proliferating cells. Additionally, Tryp-ES demonstrated effectiveness in alleviating scaling and inflammatory responses in a psoriasis mouse model. The administration of Tryp-ES in liquid was demonstrated more effective in treating psoriatic mice than those in gels. Intriguingly, lipidomics analysis has revealed that ethosomes-based supplementation with phospholipids can help repair the skin barrier and alleviate the skin symptoms associated with psoriasis. In conclusion, the microfluidic approach of preparing ethosomes is straightforward and provides a novel opportunity for enhancing the bioavailability of hydrophobic drugs and for feasible topical therapy of psoriasis.

Author contributions

RX and NL designed the processes and experiments. PW, SH, CC, SG, CW, XC, XW, PS are involved in preparing samples and performing experiments. RX, NL, PW, SH analyzed and interpreted data. RX and NL supervised the overall

Wang *et al. Journal of Nanobiotechnology*   (2024) 22:584

Page 20 of 21

research. RX, NL, PW, SH contributed to the writing of the manuscript. All authors contributed and approved the submitted version.

Data availability
No datasets were generated or analysed during the current study.

Declarations

Ethics approval and consent to participate
Not applicable.

Consent for publication
Not applicable.

Competing interests
The authors declare no competing interests.

Author details
[1]Department of Biomedical Engineering and Technology, Institute of Basic Theory for Chinese Medicine, China Academy of Chinese Medical Sciences, Beijing 100700, China
[2]Guang'anmen Hospital, China Academy of Chinese Medical Sciences, Beijing 100053, China
[3]Central Instrument Facility, Institute of Basic Theory for Chinese Medicine, China Academy of Chinese Medical Sciences, Beijing 100700, China
[4]Institute of Basic Theory for Chinese Medicine, China Academy of Chinese Medical Sciences, Beijing 100700, China
[5]Xiyuan Hospital, China Academy of Chinese Medical Sciences, Beijing 100091, China

References

1. Walter K. Psoriasis. JAMA. 2022;327(19):1936. https://doi.org/10.1001/jama.2022.5270.
2. Nestle FO, Kaplan DH, Barker J, Psoriasis. N Engl J Med. 2009;361(5):496–509. https://doi.org/10.1056/NEJMra0804595.
3. Lowes MA, Suarez-Farinas M, Krueger JG. Immunology of psoriasis. Annu Rev Immunol. 2014;32:227–55. https://doi.org/10.1146/annurev-immunol-032713-120225.
4. Boehncke WH, Schon MP, Psoriasis. Lancet. 2015;386(9997):983–94. https://doi.org/10.1016/S0140-6736(14)61909-7.
5. Griffiths CEM, Armstrong AW, Gudjonsson JE, Barker J, Psoriasis. Lancet. 2021;397(10281):1301–15. https://doi.org/10.1016/S0140-6736(20)32549-6.
6. Hawkes JE, Chan TC, Krueger JG. Psoriasis pathogenesis and the development of novel targeted immune therapies. J Allergy Clin Immunol. 2017;140(3):645–53. https://doi.org/10.1016/j.jaci.2017.07.004.
7. Dauden E, Carretero G, Rivera R, Ferrandiz C, Llamas-Velasco M, de la Cueva P, Belinchon I, Gomez-Garcia FJ, Herrera-Acosta E, Ruiz-Genao DP, et al. Long-term safety of nine systemic medications for psoriasis: a cohort study using the Spanish Registry of adverse events for Biological Therapy in Dermatological diseases (BIOBADADERM) Registry. J Am Acad Dermatol. 2020;83(1):139–50. https://doi.org/10.1016/j.jaad.2020.03.033.
8. Rapalli VK, Waghule T, Gorantla S, Dubey SK, Saha RN, Singhvi G. Psoriasis: pathological mechanisms, current pharmacological therapies, and emerging drug delivery systems. Drug Discov Today. 2020;25(12):2212–26. https://doi.org/10.1016/j.drudis.2020.09.023.
9. Rahman M, Akhter S, Ahmad J, Ahmad MZ, Beg S, Ahmad FJ. Nanomedicine-based drug targeting for psoriasis: potentials and emerging trends in nanoscale pharmacotherapy. Expert Opin Drug Deliv. 2015;12(4):635–52. https://doi.org/10.1517/17425247.2015.982088.
10. Li N, Qin Y, Dai D, Wang P, Shi M, Gao J, Yang J, Xiao W, Song P, Xu R. Transdermal Delivery of Therapeutic Compounds with Nanotechnological approaches in Psoriasis. Front Bioeng Biotechnol. 2022;9. https://doi.org/10.3389/fbioe.2021.804415.
11. Khan NR, Wong TW. 5-Fluorouracil ethosomes - skin deposition and melanoma permeation synergism with microwave. Artif Cells Nanomed Biotechnol. 2018;46(sup1):568–77. https://doi.org/10.1080/21691401.2018.1431650.
12. Peram MR, Jalalpure S, Kumbar V, Patil S, Joshi S, Bhat K, Diwan P. Factorial design based curcumin ethosomal nanocarriers for the skin cancer delivery: in vitro evaluation. J Liposome Res. 2019;29(3):291–311. https://doi.org/10.1080/08982104.2018.1556292.
13. Murakami M, Yamamoto K, Taketomi Y, Phospholipase. A(2) in skin biology: new insights from gene-manipulated mice and lipidomics. Inflamm Regen. 2018;38:31. https://doi.org/10.1186/s41232-018-0089-2. From NLM.
14. Tenchov R, Bird R, Curtze AE, Zhou Q. Lipid NanoparticlesFrom liposomes to mRNA vaccine delivery, a Landscape of Research Diversity and Advancement. ACS Nano. 2021;15(11):16982–7015. PubMedhttps://doi.org/10.1021/acsnano.1c04996.
15. Kendall AC, Nicolaou A. Bioactive lipid mediators in skin inflammation and immunity. Prog Lipid Res. 2013;52(1):141–64. https://doi.org/10.1016/j.plipres.2012.10.003.
16. Zouboulis CC, Coenye T, He L, Kabashima K, Kobayashi T, Niemann C, Nomura T, Oláh A, Picardo M, Quist SR, et al. Sebaceous immunobiology - skin homeostasis, pathophysiology, coordination of innate immunity and inflammatory response and disease associations. Front Immunol. 2022;13:1029818. PubMedhttps://doi.org/10.3389/fimmu.2022.1029818.
17. Kong Y, Jiang J, Huang Y, Liu X, Jin Z, Li L, Wei F, Liu X, Yin J, Zhang Y, et al. Narciclasine inhibits phospholipase A2 and regulates phospholipid metabolism to ameliorate psoriasis-like dermatitis. Front Immunol. 2022;13:1094375. PubMedhttps://doi.org/10.3389/fimmu.2022.1094375.
18. Feige E, Mendel I, George J, Yacov N, Harats D. Modified phospholipids as anti-inflammatory compounds. Curr Opin Lipidol. 2010;21(6):525–9. https://doi.org/10.1097/MOL.0b013e32833f2fcb.
19. Karapetyan S, Davtyan H, Khachikyan K, Hakobyan G. Impact of supplemental essential phospholipids on treatment outcome and quality of life of patients with psoriasis with moderate severity. Dermatol Ther. 2022;35(4):e15335. https://doi.org/10.1111/dth.15335.
20. Farkas A, Kemeny L. Alcohol, liver, systemic inflammation and skin: a focus on patients with psoriasis. Skin Pharmacol Physiol. 2013;26(3):119–26. https://doi.org/10.1159/000348865.
21. Fiume MM, Bergfeld WF, Belsito DV, Hill RA, Klaassen CD, Liebler D, Marks JG Jr., Shank RC, Slaga TJ, Snyder PW, et al. Safety assessment of propylene glycol, tripropylene glycol, and PPGs as used in cosmetics. Int J Toxicol. 2012;31(5 Suppl):S245–60. https://doi.org/10.1177/1091581812461381.
22. Elsayed MM, Abdallah OY, Naggar VF, Khalafallah NM. PG-liposomes: novel lipid vesicles for skin delivery of drugs. J Pharm Pharmacol. 2007;59(10):1447–50. https://doi.org/10.1211/jpp.59.10.0017.
23. Abdulbaqi IM, Darwis Y, Khan NA, Assi RA, Khan AA. Ethosomal nanocarriers: the impact of constituents and formulation techniques on ethosomal properties, in vivo studies, and clinical trials. Int J Nanomed. 2016;11:2279–304. https://doi.org/10.2147/ijn.S105016. From NLM.
24. Natsheh H, Touitou E. Phospholipid Vesicles for Dermal/Transdermal and Nasal Administration of active molecules: the Effect of surfactants and alcohols on the fluidity of their lipid bilayers and Penetration Enhancement properties. Molecules. 2020;25(13). https://doi.org/10.3390/molecules25132959.
25. Capretto L, Carugo D, Mazzitelli S, Nastruzzi C, Zhang X. Microfluidic and lab-on-a-chip preparation routes for organic nanoparticles and vesicular systems for nanomedicine applications. Adv Drug Deliv Rev. 2013;65(11–12):1496–532. PubMedhttps://doi.org/10.1016/j.addr.2013.08.002.
26. Tian F, Cai L, Liu C, Sun J. Microfluidic technologies for nanoparticle formation. Lab Chip. 2022;22(3):512–29. PubMedhttps://doi.org/10.1039/d1lc00812a.
27. Gao J, Li Z, Li J, Song P, Yang J, Xiao W, Li N, Xu R. Peptide-based HDL as an effective delivery system for lipophilic drugs to restrain Atherosclerosis Development. Int J Nanomed. 2022;17:3877–92. PubMedhttps://doi.org/10.2147/IJN.S374736.
28. Xu RD, Li SZ, Shi MF, Li ZY, Wang Y, Li J, Li Q, Klausen LH, Li A, Zhao HY et al. Peptide-based high-density lipoprotein promotes adipose tissue browning

Wang *et al. Journal of Nanobiotechnology* (2024) 22:584

Page 21 of 21

and restrains development of atherosclerosis and type 2 diabetes. *Nano Today* 2021, *36*. DOI: ARTN 101054 1.10.1016/j.nantod.2020.101054.

29. Xiong Y, Wang J, Wang S, Li H, Zhou X. Tryptanthrin ameliorates imiquimod-induced psoriasis in mice by suppressing inflammation and oxidative stress via NF-kappaB/MAPK/Nrf2 pathways. J Nat Med. 2023;77(1):188–201. https://doi.org/10.1007/s11418-022-01664-9.

30. Chang HN, Yeh YC, Chueh HY, Pang JS. The anti-angiogenic effect of tryptanthrin is mediated by the inhibition of apelin promoter activity and shortened mRNA half-life in human vascular endothelial cells. Phytomedicine. 2019;58:152879. https://doi.org/10.1016/j.phymed.2019.152879.

31. Wang P, Gao J, Guo S, Liu H, Cao C, Hong S, Sun Y, Wang C, Xiao W, Song P, et al. Benefits of topical indigo naturalis nanofibrous patch on psoriatic skin: a transdermal strategy for botanicals. Mater Today Bio. 2023;22:100756. https://doi.org/10.1016/j.mtbio.2023.100756.

32. Viegas JSR, Praça FG, Caron AL, Suzuki I, Silvestrini AVP, Medina WSG, Del Ciampo JO, Kravicz M, Bentley M. Nanostructured lipid carrier co-delivering tacrolimus and TNF-α siRNA as an innovate approach to psoriasis. Drug Deliv Transl Res. 2020;10(3):646–60. https://doi.org/10.1007/s13346-020-00723-6. From NLM.

33. Godin B, Touitou E. Ethosomes: new prospects in transdermal delivery. Crit Rev Ther Drug Carrier Syst. 2003;20(1):63–102. https://doi.org/10.1615/critrev-therdrugcarriersyst.v20.i1.20. From NLM.

34. Dayan N, Touitou E. Carriers for skin delivery of trihexyphenidyl HCl: ethosomes vs. liposomes. Biomaterials. 2000;21(18):1879–85. https://doi.org/10.1016/s0142-9612(00)00063-6.

35. Sudhakar K, Mishra V, Jain S, Rompicherla NC, Malviya N, Tambuwala MM. Development and evaluation of the effect of ethanol and surfactant in vesicular carriers on lamivudine permeation through the skin. Int J Pharm. 2021;610:121226. https://doi.org/10.1016/j.ijpharm.2021.121226.

36. Herrmann FC. Easy ultrastructural insight into the internal morphology of biological specimens by Atomic Force Microscopy. Sci Rep. 2021;11(1):10214. https://doi.org/10.1038/s41598-021-89633-2.

37. Sakran W, Abdel-Rashid RS, Saleh F, Abdel-Monem R. Ethosomal gel for rectal transmucosal delivery of domperidone: design of experiment, in vitro, and in vivo evaluation. Drug Deliv. 2022;29(1):1477–91. https://doi.org/10.1080/10717544.2022.2072542. From NLM.

38. Pemberton MA, Kimber I. Propylene glycol, skin sensitisation and allergic contact dermatitis: a scientific and regulatory conundrum. Regul Toxicol Pharmacol. 2023;138:105341. https://doi.org/10.1016/j.yrtph.2023.105341. From NLM.

39. Iizhar SA, Syed IA, Satar R, Ansari SA. In vitro assessment of pharmaceutical potential of ethosomes entrapped with terbinafine hydrochloride. J Adv Res. 2016;7(3):453–61. https://doi.org/10.1016/j.jare.2016.03.003. From NLM.

40. Yan J, Zhu J, Cui M, Zhang J, Ma F, Su Y, Han X. Multifunctional Mineral hydrogels: potential in Artificially Intelligent skins and Drug Delivery. ACS Omega. 2019;4(21):19145–52. https://doi.org/10.1021/acsomega.9b02435. From NLM.

41. Gugleva V, Michailova V, Mihaylova R, Momekov G, Zaharieva MM, Najdenski H, Petrov P, Rangelov S, Forys A, Trzebicka B, et al. Formulation and evaluation of Hybrid Niosomal in situ gel for Intravesical Co-delivery of Curcumin and Gentamicin Sulfate. Pharmaceutics. 2022;14(4). https://doi.org/10.3390/pharmaceutics14040747. From NLM.

42. Gavrieli Y, Sherman Y, Ben-Sasson SA. Identification of programmed cell death in situ via specific labeling of nuclear DNA fragmentation. J Cell Biol. 1992;119(3):493–501. PubMed.

43. Xie X, Cui Q, Jiang T, Zhao Z, Liu Z, Liu J, Yao Q, Wang Y, Dang E, Wang G, et al. A critical role of endothelial Skp2/PTEN Axis in Angiogenesis and Psoriasis. Br J Dermatol. 2023. https://doi.org/10.1093/bjd/ljad399.

44. Han Q, Niu X, Hou R, Li J, Liu Y, Li X, Li J, Li Y, Zhang K, Wu Y. Dermal mesenchymal stem cells promoted adhesion and migration of endothelial cells by integrin in psoriasis. Cell Biol Int. 2021;45(2):358–67. https://doi.org/10.1002/cbin.11492.

45. Yao Q, Zhai YY, He Z, Wang Q, Sun L, Sun T, Lv L, Li Y, Yang J, Lv D, et al. Water-responsive gel extends drug retention and facilitates skin penetration for curcumin topical delivery against psoriasis. Asian J Pharm Sci. 2023;18(2):100782. https://doi.org/10.1016/j.ajps.2023.100782.

46. Vasowala T, Gharat S, Mhase M, Momin M. Advances in hydrogels based cutaneous drug delivery system for management of psoriasis. Eur Polymer J. 2024;202:112630. https://doi.org/10.1016/j.eurpolymj.2023.112630.

47. Hallan SS, Sguizzato M, Mariani P, Cortesi R, Huang N, Simelière F, Marchetti N, Drechsler M, Ruzgas T, Esposito E. Design and Characterization of Ethosomes for Transdermal Delivery of Caffeic Acid. *Pharmaceutics* 2020, *12* (8). DOI: 10.3390/pharmaceutics12080740 From NLM.

48. Elsayed MM, Abdallah OY, Naggar VF, Khalafallah NM. Deformable liposomes and ethosomes: mechanism of enhanced skin delivery. Int J Pharm. 2006;322(1–2):60–6. https://doi.org/10.1016/j.ijpharm.2006.05.027. From NLM.

49. Park SH, Shin HS, Park SN. A novel pH-responsive hydrogel based on carboxymethyl cellulose/2-hydroxyethyl acrylate for transdermal delivery of naringenin. Carbohydr Polym. 2018;200:341–52. https://doi.org/10.1016/j.carbpol.2018.08.011. From NLM.

50. Knox S, O'Boyle NM. Skin lipids in health and disease: a review. Chem Phys Lipids. 2021;236:105055. PubMedhttps://doi.org/10.1016/j.chemphyslip.2021.105055.

51. Simard M, Morin S, Ridha Z, Pouliot R. Current knowledge of the implication of lipid mediators in psoriasis. Front Immunol. 2022;13:961107. PubMedhttps://doi.org/10.3389/fimmu.2022.961107.

52. Snekvik I, Nilsen TIL, Romundstad PR, Saunes M. Metabolic syndrome and risk of incident psoriasis: prospective data from the HUNT study, Norway. Br J Dermatol. 2019;180(1):94–9. PubMedhttps://doi.org/10.1111/bjd.16885.

53. Coderch L, López O, de la Maza A, Parra JL. Ceramides and skin function. Am J Clin Dermatol. 2003;4(2):107–29. PubMed.

54. Mijaljica D, Townley JP, Spada F, Harrison IP. The heterogeneity and complexity of skin surface lipids in human skin health and disease. Prog Lipid Res. 2024;93:101264. PubMedhttps://doi.org/10.1016/j.plipres.2023.101264.

55. Tessema EN, Gebre-Mariam T, Neubert RHH, Wohlrab J. Potential applications of Phyto-Derived ceramides in improving epidermal barrier function. Skin Pharmacol Physiol. 2017;30(3):115–38. https://doi.org/10.1159/000464337. PubMed.

56. Li Q, Fang H, Dang E, Wang G. The role of ceramides in skin homeostasis and inflammatory skin diseases. J Dermatol Sci. 2020;97(1):2–8. PubMedhttps://doi.org/10.1016/j.jdermsci.2019.12.002.

57. Rudd AK, Devaraj NK, Rudd AK, Devaraj NK. Traceless synthesis of ceramides in living cells reveals saturation-dependent apoptotic effects. Proc Natl Acad Sci. 2018-7-17;115(29). https://doi.org/10.1073/pnas.1804266115.

Publisher's note